

# Learning to Bound: A Generative Cramér-Rao Bound

Hai Victor Habi, Hagit Messer, Life Fellow, IEEE and Yoram Bresler, Life Fellow, IEEE

**Abstract**—The Cramér-Rao bound (CRB), a well-known lower bound on the performance of any unbiased parameter estimator, has been used to study a wide variety of problems. However, to obtain the CRB, requires an analytical expression for the likelihood of the measurements given the parameters, or equivalently a precise and explicit statistical model for the data. In many applications, such a model is not available. Instead, this work introduces a novel approach to approximate the CRB using data-driven methods, which removes the requirement for an analytical statistical model. This approach is based on the recent success of deep generative models in modeling complex, high-dimensional distributions. Using a learned normalizing flow model, we model the distribution of the measurements and obtain an approximation of the CRB, which we call Generative Cramér-Rao Bound (GCRB). Numerical experiments on simple problems validate this approach, and experiments on two image processing tasks of image denoising and edge detection with a learned camera noise model demonstrate its power and benefits.

**Index Terms**—Generative Models, Normalizing Flows, CRB, Estimation.

## I. INTRODUCTION

The Cramér-Rao Bound (CRB) is a lower bound on the variance of any unbiased parameter estimator [1]–[3]. It has been used in a wide variety of estimation problems such as DOA [4], TDOA [5], etc. The CRB enables to understand the fundamental limits in a given parameter estimation problem, regardless of the algorithm used. However, to obtain an applicable CRB, it is required to have an analytical expression for the likelihood of the measurements given the parameters, or equivalently a precise and explicit statistical model for the measurements. In many applications, such a model is not available. Examples include device-specific noise statistics, such as in image sensors [6], or radio frequency communications with jamming [7] or unknown channel characteristics [8].

Recently, generative models have shown state-of-the-art results in modeling complex, high-dimensional data distribution from images [9], [10], voice [11], image noise [6] and communications channels [12]. In this work, we suggest to use generative models to learn the measurement distribution from data. Then, using this generative model, we obtain an approximation to the CRB. We call this approach a *Generative Cramér-Rao Bound (GCRB)* and show conditions under which the GCRB accurately

approximates the CRB. Specifically, we use a normalizing flow [13], [14] to learn a generative model for the measurement distribution. This is used, in turn, to generate samples of the gradient of the log-likelihood and obtain, as an empirical mean, an estimate of the Fisher Information Matrix (FIM). We refer to this estimate as a *Generative Fisher Information Matrix (GFIM)*. Finally, by inverting the GFIM, we obtain the GCRB. To assess the sampling requirements for the estimation of the GCRB, we derive a bound on the error in the GCRB due to the use of an empirical mean.

To validate the GCRB, we examine two simple examples of parameter estimation with a Gaussian and non-Gaussian measurement distributions, respectively. First, we show analytically that the GCRB and the CRB produce the same results under optimal conditions, i.e., assuming an invertible generative model that produces the exact measurement distribution. Second, we illustrate a realistic setup where we train a standard normalizing flow on each of the two measurement distributions to evaluate its GCRB and compare it to the corresponding CRB.

Then, to demonstrate the value of GCRB, we use two examples from image processing: image denoising, and edge position detection, in the presence of realistic, camera-specific noise. We model the camera noise using a recently published normalizing flow model NoiseFlow [6]. With these examples, we show two main benefits of the GCRB: (1) a lower bound for image denoising for several cameras, which provides a device-specific lower bound; and (2) we compare the GCRB lower bound on edge position detection to the CRB that would be obtained using two popular noise models: white Gaussian, and Noise Level Function (NLF) noises. This experiment demonstrates that the analytical CRB with specific assumed noise models (such as the white Gaussian or even the refined NLF noise models) cannot capture the complex actual noise of image sensors and its effect on image processing performance, which is however successfully captured by the proposed GCRB.

The main contributions of this paper are the following.

- We introduce a Generative Cramér-Rao Bound - a data-driven approach to approximate the CRB, eliminating the need for an analytical statistical data model.
- We demonstrate the benefit of the GCRB on two real-world problem of image denoising and edge detection.
- We evaluate the approximation quality (between the CRB and the GCRB) using two simple measurement distributions.

H.V. Habi and H. Messer are with the School of Electrical Engineering, Tel Aviv University, Tel Aviv 69978, Israel (e-mail: haivictorh@mail.tau.ac.il; messer@eng.tau.ac.il).

Y. Bresler is with the Department of Electrical and Computer Engineering, University of Illinois, Urbana-Champaign, USA (e-mail: ybresler@illinois.edu).

- We provide a theoretical bound on the GCRB error due to empirical sampling.

In the spirit of reproducible research, we make the code and trained models of the generative Cramér-Rao bound available online [15].

The paper is organized as follows: the Generative Cramér-Rao Bound is developed in Sec. II followed by a brief overview of normalizing flows in Sec. III. In Sec. IV we present a set of parameter estimation examples, including simple parameter estimation in Gaussian and Non-Gaussian noise, and image processing with device-specific noise. The experimental results for the GCRB are described in Sec. V, and Sec. VI provides discussion and conclusions. Appendices are included in the online Supplementary Material.

## II. GENERATIVE CRAMER-RAO BOUND

We introduce the Generative Cramér-Rao Bound (GCRB), a data-driven approach to approximate the Cramér-Rao Bound (CRB). We begin with the measurements model, the classical CRB, and problem statement. Then, we introduce our method to obtain the Generative Fisher Information Matrix (GFIM) and the GCRB using an invertible generative model. We state sufficient conditions for the convergence of the GCRB to the CRB, and bound the relative error of the GCRB due to estimation of the expected value by a sample mean.

### A. Data model and Problem Definition

Consider a data model described by random mapping, also known as a "channel," producing a random measurement  $\mathbf{R}(\boldsymbol{\theta})$  from a deterministic input  $\boldsymbol{\theta}$ . The channel is fully characterized by the probability density function (PDF)  $p_{\mathbf{R}}(\mathbf{r}; \boldsymbol{\theta})$ . Formally, let  $\boldsymbol{\theta} \in \mathbb{R}^k$  be a parameter vector,  $\mathbf{R} \in \mathbb{R}^d$  the measurement vector, and  $p_{\mathbf{R}}(\cdot; \boldsymbol{\theta}) : \mathbb{R}^d \rightarrow \mathbb{R}$  the probability density function of  $\mathbf{R}$  for a given parameter value  $\boldsymbol{\theta}$ . The CRB is specified in terms of the negative log-likelihood (NLL) of  $\mathbf{R}$  given  $\boldsymbol{\theta}$

$$L_{\mathbf{R}}(\boldsymbol{\theta}) \triangleq -\log p_{\mathbf{R}}(\mathbf{r}; \boldsymbol{\theta})$$

and the corresponding Fisher information matrix (FIM)

$$\mathbf{F}_{\mathbf{R}}(\boldsymbol{\theta}) \triangleq \mathbb{E}_{\mathbf{R}} \left[ \frac{\partial L_{\mathbf{R}}(\boldsymbol{\theta})}{\partial \boldsymbol{\theta}} \left[ \frac{\partial L_{\mathbf{R}}(\boldsymbol{\theta})}{\partial \boldsymbol{\theta}} \right]^T \right], \quad (1)$$

where  $\mathbb{E}_{\mathbf{R}}[\cdot]$  denotes the expectation with respect to  $\mathbf{R}$ . For the CRB to apply, we assume that appropriate regularity conditions [2], [16] hold. We list below those to which we appeal in this paper explicitly, with the understanding that the remaining regularity conditions hold too.

*Assumption 2.1:*  $p_{\mathbf{R}}(\mathbf{r}; \boldsymbol{\theta})$  satisfies the following conditions:

- A.1 For all  $\boldsymbol{\theta} \in \Theta$ , where  $\Theta$  is an open set, the densities  $p_{\mathbf{R}}(\mathbf{r}; \boldsymbol{\theta})$  have a common support  $\Upsilon = \{\mathbf{r} : p_{\mathbf{R}}(\mathbf{r}; \boldsymbol{\theta}) > 0\} \subseteq \mathbb{R}^d$  that is independent of  $\boldsymbol{\theta}$ .
- A.2 For any  $\mathbf{r} \in \Upsilon$  and  $\boldsymbol{\theta} \in \Theta$  the derivative (gradient)  $\frac{\partial p_{\mathbf{R}}(\mathbf{r}; \boldsymbol{\theta})}{\partial \boldsymbol{\theta}}$  with respect to  $\boldsymbol{\theta}$  exists and is finite.

A.3 For all  $\boldsymbol{\theta} \in \Theta$ , the FIM is positive definite,  $\mathbf{F}_{\mathbf{R}} \succ 0$ .

Let  $\hat{\boldsymbol{\theta}}(\mathbf{R})$  be an unbiased estimator of  $\boldsymbol{\theta}$  from the measurement  $\mathbf{R}(\boldsymbol{\theta})$  that satisfies  $\mathbb{E}_{\mathbf{R}}[\|\hat{\boldsymbol{\theta}}(\mathbf{R})\|_2^2] < \infty$ . Then the covariance matrix of any such estimator of  $\boldsymbol{\theta}$  satisfies the so-called *information inequality*

$$\mathbb{E}_{\mathbf{R}}[\hat{\boldsymbol{\theta}}(\mathbf{R})\hat{\boldsymbol{\theta}}(\mathbf{R})^T] \succ \text{CRB}_{\mathbf{R}}(\boldsymbol{\theta}) \triangleq [\mathbf{F}_{\mathbf{R}}(\boldsymbol{\theta})]^{-1}, \quad (2)$$

In (2) the inequality  $A \succ B$  for matrices  $A$  and  $B$  means that  $A - B \succ 0$ .

We wish to determine  $\text{CRB}_{\mathbf{R}}(\boldsymbol{\theta})$  when the channel pdf  $p_{\mathbf{R}}(\mathbf{r}; \boldsymbol{\theta})$  is unknown, and we are instead given representative data samples. We define this problem as follows.

*Problem 1:* Let  $\Theta \subseteq \mathbb{R}^k$  be an open set. Assume that  $p_{\mathbf{R}}(\mathbf{r}; \boldsymbol{\theta})$  and  $p_{\boldsymbol{\theta}}(\boldsymbol{\theta})$  satisfy Assumptions 2.1 and 2.2. Given a data set  $\mathcal{D} = \{\boldsymbol{\theta}_i, \mathbf{R}_i\}_{i=1}^l$  of  $l$  channel input-output samples that are independent and identically-distributed (i.i.d) as  $\mathbf{R}_i \sim p_{\mathbf{R}}(\mathbf{r}; \boldsymbol{\theta}_i)$ ,  $\boldsymbol{\theta}_i \sim p(\boldsymbol{\theta})$ , obtain an approximation to the Cramér-Rao lower bound on the estimation of parameter  $\boldsymbol{\theta} \in \Theta$  from the measurement  $\mathbf{R}(\boldsymbol{\theta})$ :

$$\text{CRB}_{\mathbf{R}}(\boldsymbol{\theta}) \quad \forall \boldsymbol{\theta} \in \Theta.$$

The additional assumptions indicated above in Problem 1 are the following.

*Assumption 2.2:*

- A.4  $\Theta$  is bounded set.
- A.5  $p(\boldsymbol{\theta}) > \epsilon_{\Theta} > 0 \quad \forall \boldsymbol{\theta} \in \Theta$
- A.6  $\Upsilon$  is connected set.

Assumptions 2.1 are required in Problem 1 for the validity of the information inequality. Assumptions 2.2 facilitate the training of the normalizing flow and generator. Specifically, A.6 facilitates the universal approximation of the generator; and A.4 and A.5 enable all  $\boldsymbol{\theta} \in \Theta$  to be present in the training set with some non-vanishing probability, and limit the degree of generalization to unseen  $\boldsymbol{\theta}$  required of the generator. Note that while  $\boldsymbol{\theta}$  is a deterministic unknown parameter for the purposes of the CRB,  $p(\boldsymbol{\theta})$  describes the *sampling* distribution of the training set  $\mathcal{D}$ . We will address these assumptions where relevant.

### B. Method

We address Problem 1 with a two-stage approach. In the first stage, we train a conditional normalizing flow (invertible neural network) that learns the distribution of the measurements. Training of normalizing flows is a well-studied subject, and we only provide a short overview in Section III. In the second stage, we obtain an approximation of the CRB from the trained conditional normalizing flow.

In the rest of this section, we describe how to approximate the CRB using a trained conditional normalizing flow. Let  $\nu(\boldsymbol{\gamma}; \boldsymbol{\theta})$  be a trained conditional normalizing flow with conditioning input  $\boldsymbol{\theta}$  and data input  $\boldsymbol{\gamma}$ . Then  $\mathbf{G}(\mathbf{z}; \boldsymbol{\theta})$ , the inverse of  $\nu$  with respect to  $\boldsymbol{\gamma}$ , is a conditional generator with conditioning input  $\boldsymbol{\theta}$  and random input

$\mathbf{z}$  with known and tractable distribution (usually  $\mathbf{z} \sim \mathcal{N}(\mathbf{0}, \mathbf{I})$ ), producing the output:

$$\Gamma(\boldsymbol{\theta}) = \mathbf{G}(\mathbf{z}; \boldsymbol{\theta}). \quad (3)$$

While  $\mathbf{G}$  is usually obtained directly from  $\nu$  by a simple transformation and does not require separate training (see Sec. III), we refer to  $\mathbf{G}$  as a *trained generator* because it is obtained from the trained normalizing flow  $\nu$ . We assume (in a sense soon to be made precise) that the trained generator simulates the random measurement process  $\mathbf{R}(\boldsymbol{\theta})$  accurately, i.e.  $\Gamma(\boldsymbol{\theta})$  has the same distribution as  $\mathbf{R}(\boldsymbol{\theta})$ .

We make the standard assumption that for each  $\boldsymbol{\theta}$ ,  $\mathbf{G}(\cdot; \boldsymbol{\theta}) : \mathbb{R}^d \mapsto \mathbb{R}^d$  is a bijection, i.e., it has an inverse  $\nu(\cdot; \boldsymbol{\theta})$ , and that both are differentiable functions, that is, for each  $\boldsymbol{\theta}$ , the mapping  $\mathbf{G}(\cdot; \boldsymbol{\theta})$  is a diffeomorphism. Furthermore, for reasons explained below, we strengthen the differentiability assumption to  $\mathbf{G} \in C^2$ , that is the first and second order derivatives, including the mixed derivative of  $\mathbf{G}$  w.r.t  $\mathbf{z}$  and  $\boldsymbol{\theta}$  exist and are continuous. A trained  $\mathbf{G}$  is a deterministic function of  $\boldsymbol{\theta}$  and  $\mathbf{z}$ , implemented as a neural network  $\mathbf{G}(\cdot; \boldsymbol{\theta})$  that is invertible in its first parameter. Thanks to the randomness of  $\mathbf{z}$ , the generative model (3) is a random mapping from  $\boldsymbol{\theta}$  to  $\Gamma(\boldsymbol{\theta})$ .

It follows, using the standard formula of transformation of random variables, that the probability density function of  $\Gamma(\boldsymbol{\theta})$  is

$$p_\Gamma(\boldsymbol{\gamma}; \boldsymbol{\theta}) = p_{\mathbf{z}}(\nu(\boldsymbol{\gamma}; \boldsymbol{\theta})) |\det \mathbf{J}_\nu(\boldsymbol{\gamma}; \boldsymbol{\theta})|, \quad (4)$$

where  $\mathbf{J}_\nu(\boldsymbol{\gamma}; \boldsymbol{\theta}) = \frac{\partial \nu(\boldsymbol{\gamma}; \boldsymbol{\theta})}{\partial \boldsymbol{\gamma}}$  is the Jacobian matrix of the transformation  $\nu(\boldsymbol{\gamma}; \boldsymbol{\theta})$  with respect to  $\boldsymbol{\gamma}$ , and  $\det \mathbf{A}$  denotes the determinant of matrix  $\mathbf{A}$ . Since both  $\mathbf{G}$  and  $\nu$  are known functions and the pdf of  $\mathbf{z}$  is known (standard normal), in principle, the pdf  $p_\Gamma(\boldsymbol{\gamma}; \boldsymbol{\theta})$  can be determined.

Given the trained normalizing flow  $\nu$  and the corresponding generator  $\mathbf{G}$ , we compute the GCRB as follows. First using (4) we determine (as detailed in Appendix A.1) the so-called score vector

$$\begin{aligned} \mathbf{s}_\theta(\mathbf{z}) &\triangleq \left. \frac{\partial \log p_\Gamma(\boldsymbol{\gamma}; \boldsymbol{\theta})}{\partial \boldsymbol{\theta}} \right|_{\boldsymbol{\gamma}=\mathbf{G}(\mathbf{z}; \boldsymbol{\theta})} \\ &= \left. \frac{\partial \log [p_{\mathbf{z}}(\nu(\boldsymbol{\gamma}; \boldsymbol{\theta})) |\det \mathbf{J}_\nu(\boldsymbol{\gamma}; \boldsymbol{\theta})|]}{\partial \boldsymbol{\theta}} \right|_{\boldsymbol{\gamma}=\mathbf{G}(\mathbf{z}; \boldsymbol{\theta})} \end{aligned} \quad (5)$$

$$= \left. \frac{\partial \nu(\boldsymbol{\gamma}; \boldsymbol{\theta})}{\partial \boldsymbol{\theta}} \right|_{\boldsymbol{\gamma}=\mathbf{G}(\mathbf{z}; \boldsymbol{\theta})}^T \times \left. \frac{\partial \log p_{\mathbf{z}}(\mathbf{z})}{\partial \mathbf{z}} + \mathbf{k}(\boldsymbol{\gamma}, \boldsymbol{\theta}) \right|_{\boldsymbol{\gamma}=\mathbf{G}(\mathbf{z}; \boldsymbol{\theta})}, \quad (6)$$

$$\text{where } [\mathbf{k}(\boldsymbol{\gamma}, \boldsymbol{\theta})]_i = \text{Tr} \left( \mathbf{J}_\nu^{-1}(\boldsymbol{\gamma}; \boldsymbol{\theta}) \frac{\partial \mathbf{J}_\nu(\boldsymbol{\gamma}; \boldsymbol{\theta})}{\partial \theta_i} \right), \quad (7)$$

with  $\text{Tr}(\mathbf{A})$  denoting the trace of matrix  $\mathbf{A}$ . In (6),  $\frac{\partial \nu(\boldsymbol{\gamma}; \boldsymbol{\theta})}{\partial \boldsymbol{\theta}}$  is the Jacobian matrix of  $\nu$  w.r.t  $\boldsymbol{\theta}$ , and in (7)  $\frac{\partial \mathbf{J}_\nu(\boldsymbol{\gamma}; \boldsymbol{\theta})}{\partial \theta_i}$  is a derivative matrix of the Jacobian matrix  $\mathbf{J}_\nu$  w.r.t the  $i$ -th component of  $\boldsymbol{\theta}$ . Note that to evaluate the score vector for a given  $\mathbf{z}$  both  $\mathbf{G}$  and  $\nu$  are used. We therefore refer to Formula (6) as a hybrid score vector. As an alternative, we show in Appendix A.2 an equivalent form that only uses the generator  $\mathbf{G}$ .

To perform the computation in (6)-(7) we need to be able to evaluate the following derivatives:  $\nu$  w.r.t  $\boldsymbol{\theta}$ ,  $\nu$  w.r.t  $\mathbf{z}$ , and a mixed second derivative of  $\nu$  w.r.t to  $\mathbf{z}$  and  $\boldsymbol{\theta}$ . As elaborated in Appendix A.2, this motivates the differentiability conditions imposed on  $\mathbf{G}$  above. We also require that the log-likelihood of the base distribution  $p_{\mathbf{z}}(\mathbf{z})$  be differentiable, which is satisfied by the Gaussian distribution.

As a practical matter, because  $\nu$  and  $\mathbf{G}$  are implemented as a neural networks, the required derivatives of  $\nu$  and  $\mathbf{G}$  w.r.t to their respective inputs  $\boldsymbol{\gamma}$ ,  $\mathbf{z}$  and  $\boldsymbol{\theta}$  can be easily evaluated in common deep learning frameworks such as PyTorch [17], TensorFlow, etc.

Given the score vector, we compute the Generative Fisher Information Matrix (GFIM):

$$\mathbf{F}_G(\boldsymbol{\theta}) \triangleq \mathbb{E}_{\mathbf{z}} [\mathbf{s}_\theta(\mathbf{z}) \mathbf{s}_\theta(\mathbf{z})^T]. \quad (8)$$

In practice, to avoid integration in (8), the expected value with respect to  $\mathbf{z}$  is estimated as an empirical mean by sampling from  $p_{\mathbf{z}}$ . The result is an empirical Generative Fisher Information Matrix (eGFIM) that is computed as

$$\overline{\mathbf{F}}_G(\boldsymbol{\theta}) \triangleq \frac{1}{m} \sum_{i=1}^m \mathbf{s}_\theta(\mathbf{z}_i) \mathbf{s}_\theta(\mathbf{z}_i)^T, \quad (9)$$

using  $m$  samples  $\mathbf{z}_i \sim p_{\mathbf{z}}$ . Finally, we approximate the CRB using the empirical estimate of the GCRB (eGCRB)  $\overline{\text{GCRB}}_G$  associated with generator  $\mathbf{G}$  by

$$\overline{\text{GCRB}}_G(\boldsymbol{\theta}) = \overline{\mathbf{F}}_G(\boldsymbol{\theta})^{-1}. \quad (10)$$

Given the trained neural networks  $\mathbf{G}$  and  $\nu$ , the computation of  $\overline{\text{GCRB}}_G$  for a given value of  $\boldsymbol{\theta}$  is illustrated in Fig. 1. It involves  $m$  uses of the neural networks  $\mathbf{G}$  (to generate  $\boldsymbol{\gamma}$ ) and  $\nu$  (to generate the various derivatives) and the simple computations in (6)-(7), (9), and (10), so can be computationally cheap.

In the rest of this section, we address conditions to obtain a well-trained generator (Assumption 2.4) and an associated modification of GCRB. Since in practice we have a finite dataset and a network of finite complexity, we need to bound the region  $\hat{\Upsilon}$  where generated samples can be trusted. We define this region by its assumed properties.

*Assumption 2.3 (Trusted Region):*

A.7  $\hat{\Upsilon} \subseteq \Upsilon$  is a connected and closed and bounded (hence compact) set.

A.8  $\hat{\Upsilon}$  is large enough that for some chosen  $\epsilon_r \geq 0$

$$\int_{\mathbf{r} \notin \hat{\Upsilon}} p_{\mathbf{R}}(\mathbf{r}; \boldsymbol{\theta}) d\mathbf{r} \leq \epsilon_r \quad \forall \boldsymbol{\theta} \in \Theta.$$

A.9  $p_{\mathbf{R}}(\mathbf{r}; \boldsymbol{\theta}) > \epsilon > 0 \quad \forall \mathbf{r} \in \hat{\Upsilon}$ .

To ensure that the computation of the GCRB is performed using a sample generated on the trusted region, we add an optional trimming step that removes un-trusted generated samples  $\boldsymbol{\gamma} = \mathbf{G}(\mathbf{z}) \notin \hat{\Upsilon}$ . The trimming step ensures that only values of  $\mathbf{z}$  that correspond to trusted  $\boldsymbol{\gamma} \in \hat{\Upsilon}$  are used in the computation of GCRB. By Assumption 2.3 the effect of this trimming on the approximation quality should be a negligible. Furthermore, assumption

A.9 enables all  $\mathbf{r} \in \hat{\Upsilon}$  to be present in the training set with some non-vanishing probability. Algorithm 1 describes the evaluation of the eGCRB, with the trimming step included.

---

**Algorithm 1** eGCRB Sampling

---

**Require:**  $G, \nu, B, \hat{\mathbf{r}}, m, \theta$   
 $S \leftarrow \emptyset$   
**while**  $|S| < m$  **do**  
     $\mathbf{z} \sim p_{\mathbf{Z}}(\mathbf{z})$   
     $\gamma = G(\mathbf{z}; \theta)$  ▷ Generator Step  
    **if**  $\gamma \in \hat{\Upsilon}$  **then** ▷ Timming Step  
         $\hat{\mathbf{s}} = \mathbf{s}_{\theta}(\mathbf{z})$  ▷ Compute score vector (5).  
         $S \leftarrow S \cup \{\hat{\mathbf{s}}\}$  ▷ Append to  $\hat{\mathbf{s}}$  to score set.  
    **end if**  
**end while**  
 $F_G(\theta) = \frac{1}{m} \sum_{\hat{\mathbf{s}} \in S} \hat{\mathbf{s}}^T \hat{\mathbf{s}}$  ▷ Compute eGFIM  
 $\overline{\text{GCRB}}_G(\theta) = F_G(\theta)^{-1}$  ▷ Invert eGFIM to obtain eGCRB

---

The trimming step, in the spirit of standard trimmed mean computation in robust statistics [18], is a kind of outlier removal step, which is a well-studied but also active field of research (cf. [19], [20] and the references therein). We propose a simple heuristic trimming criterion; a more refined criterion may improve the eGCRB accuracy when only limited training data is available. The trimming process consist of two steps. First, we evaluate the mean  $\bar{\mathbf{r}}$  and an upper bound  $B$  on the spread of  $\mathbf{r}$  in the training set  $\mathcal{D}$ :

$$\bar{\mathbf{r}} = \frac{1}{|\mathcal{D}|} \sum_i \mathbf{r}_i,$$

$$B = \max_i \|\mathbf{r}_i - \bar{\mathbf{r}}\|.$$

Then, the trusted set is defined as

$$\hat{\Upsilon} = \{\gamma \in \Upsilon : \|\gamma - \bar{\mathbf{r}}\| \leq B\}.$$

This trimming is designed to exclude samples  $\gamma = G(\mathbf{z})$  generated in regions where no training samples were available to train the normalizing flow. This will reduce the requirement of the normalizing flow and generator to extrapolate during inference outside the coverage of the training set. Note that thanks to the adaptivity of  $\hat{\Upsilon}$  to the training set, as the size of the training set  $|\mathcal{D}| \rightarrow \infty$ , the "unrepresented probability" vanishes:  $\epsilon_r \rightarrow 0$ .

### C. Theoretical properties

This section addresses two questions: (i) When does the generative model and proposed approach produce the correct CRB? (ii) What is the error introduced by using an empirical mean to estimate the GFIM? Our key assumption is that the generative model is expressive enough and the training data set has sufficient diversity of values of  $\theta$  and  $\mathbf{r}$  and the training is successful, resulting in a generative model that simulates the random mapping  $\mathbf{R}(\theta)$  perfectly, that is, its output has the exact parametrized distribution.

*Assumption 2.4 (Well Trained):*

$$p_{\Gamma}(\mathbf{r}; \theta) = p_{\mathbf{R}}(\mathbf{r}; \theta) \quad \forall \theta \in \Theta, \forall \mathbf{r} \in \hat{\Upsilon} \subseteq \Upsilon. \quad (11)$$

Two conditions are required for a well-trained generator (Assumption 2.4) to be realizable: (i) the generator is capable of approximating the distribution  $p_{\mathbf{R}}(\mathbf{r}; \theta)$  on  $\hat{\Upsilon}$  for each  $\theta \in \Theta$ ; and (ii) the generator can be trained to achieve this approximation using the training data. Assuming that Condition (i) holds, then Condition (ii) can be satisfied, i.e., a well-trained generator is realizable on a trusted region (Assumption 2.3) in the limit of infinite training data set if Assumption A.1 and A.6 on the measurement distribution  $p_{\mathbf{R}}(\mathbf{r}; \theta)$  and assumption A.4 on the training set distribution are satisfied.

The question of Condition (i) is an active research area, with recent results [14], [21]–[24] showing that for certain architectural choices and under some additional assumptions, normalizing flows can provide universal approximations with arbitrarily small error. As the currently available universal approximation conditions are sufficient conditions, we expect that ongoing research will result in further relaxation of the conditions and a larger variety of architectural choices.

Based on Assumption 2.4 we show that the generator will provide the same CRB as the data distribution. First, we address the case of measurements distributions bounded to a trusted region, and then we address the case of unbounded measurements distributions.

**1) Bounded Measurement Distribution:** In the case of measurements that have a distribution inherently supported on a trusted region we assume no trimming and that the set  $\Upsilon$  meets Assumption 2.3 with  $\epsilon_r = 0$ , i.e.,  $\hat{\Upsilon} = \Upsilon$ . Then, we have

*Theorem 2.1 (Exact GFIM):* Let  $G$  be a well trained normalizing flow (11) with  $\hat{\Upsilon} = \Upsilon$ . Then

$$F_G(\theta) = F_{\mathbf{R}}(\theta) \quad \forall \theta \in \Theta. \quad (12)$$

*Proof:* The result is an immediate corollary of the more general Theorem 2.3 for the case  $\hat{\Upsilon} = \Upsilon$ , because then  $\epsilon_t = 0$ , and (15) reduces to (12). ■

Theorem 2.1 states that if  $G$  is well trained, then the expectation of the eGFIM is equal to the data FIM.

The following result addresses the effects of sampling on the eGFIM.

*Corollary 1.1:*

$$\overline{\text{GCRB}}_G(\theta) \xrightarrow{m \rightarrow \infty} \text{CRB}_{\mathbf{R}}(\theta) \quad \text{a.s.}$$

*Proof:* By the strong Law of Large numbers  $\lim_{m \rightarrow \infty} \overline{F}_G(\theta) = F_G(\theta)$  a.s. Combining this with (12) and inverting yields the result. ■

It follows that if Assumption 2.4 holds then the eGCRB converges to the CRB almost surely as  $m \rightarrow \infty$ .

Next, we study the effects of finite number of samples in (9) on the accuracy of the eGCRB by deriving an upper bound on the relative error.

*Theorem 2.2 (Sampling Error):* Let  $\overline{F}_G(\theta)^{-1}$  be the eGCRB computed using a well-trained generator  $G \in \mathcal{C}^2$  (11) and it's inverse  $\nu$ . Assume that Assumption 2.3 holds



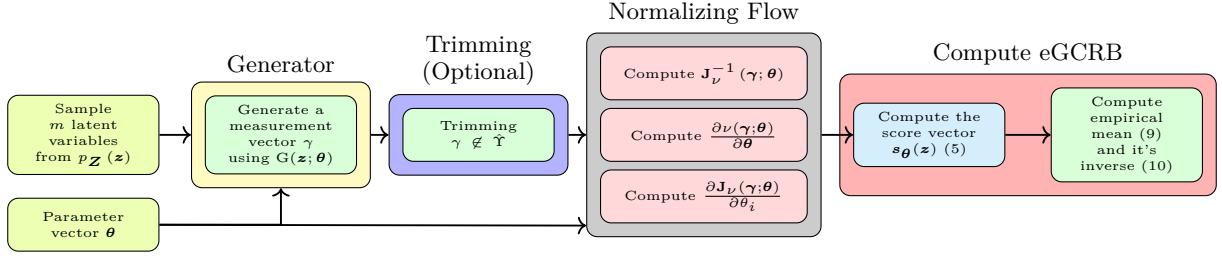


Fig. 1: Generative Cramer Rao bound using normalizing flow

with  $\epsilon_r = 0$ , and the CRB is bounded in Frobenius norm,  $\|\mathbf{F}_R(\boldsymbol{\theta})^{-1}\|_F \leq C_F(\boldsymbol{\theta})$ . Then (i) the score vector is bounded  $\|\mathbf{s}_\theta(\mathbf{z})\|_F \leq C_s(\boldsymbol{\theta})$ ; and (ii) there exist absolute constants  $C_1 > 0$  and  $C_2 > 0$  such that provided that  $m > C_1(1+u)C_F(\boldsymbol{\theta})^2$ , for any  $u > 0$  we have, with probability at least  $1 - \exp(-u)$ :

$$\text{RE}(\boldsymbol{\theta}) \triangleq \frac{\|\overline{\mathbf{F}}_G(\boldsymbol{\theta})^{-1} - \mathbf{F}_R(\boldsymbol{\theta})^{-1}\|_F}{\|\mathbf{F}_R(\boldsymbol{\theta})^{-1}\|_F} \leq C_2 \|\mathbf{F}_R(\boldsymbol{\theta})^{-1}\|_F C_s(\boldsymbol{\theta})^2 \sqrt{\frac{1+u}{m}}. \quad (13)$$

Theorem 2.2 (proved in Appendix D) is based on a bound for the precision matrix [25] and properties of the score vector. This result show that the score vector is bounded in 2-norm, and that the relative error of the eGCRB is bounded in terms of the latter bound, the CRB itself, and the number of samples. Importantly, Theorem 2.2 shows that the error decreases (at the best possible rate) as the number  $m$  of samples increases.

**2) Unbounded Measurement Distribution:** In this part we address the case of measurement distribution with unbounded support, with trimming of the generator, meaning that  $\hat{\Upsilon}$  is a strict subset of  $\Upsilon$ . Define

$$\hat{\mathbf{F}}_G(\boldsymbol{\theta}) \triangleq \int_{\hat{\mathcal{Z}}} \mathbf{s}_\theta(\mathbf{z}) \mathbf{s}_\theta(\mathbf{z})^T p_{\mathbf{Z}}(\mathbf{z}) d\mathbf{z}, \quad (14)$$

as the result of the GFIM calculation over the trimmed sample set  $\hat{\mathcal{Z}} = \{\mathbf{z} : \mathbf{G}(\mathbf{z}; \boldsymbol{\theta}) \in \hat{\Upsilon}\}$ . Then we have the following result.

**Theorem 2.3 (Trimming Error):** Let  $\mathbf{G}$  be a well-trained normalizing flow (11). Then,

$$\hat{\mathbf{F}}_G(\boldsymbol{\theta}) = \mathbf{F}_R(\boldsymbol{\theta}) - \epsilon_t(\boldsymbol{\theta}) \quad \forall \boldsymbol{\theta} \in \Theta, \quad (15)$$

where

$$\epsilon_t(\boldsymbol{\theta}) = \int_{\Upsilon \setminus \hat{\Upsilon}} \frac{\partial \mathbf{L}_R(\mathbf{r}; \boldsymbol{\theta})}{\partial \boldsymbol{\theta}} \left[ \frac{\partial \mathbf{L}_R(\mathbf{r}; \boldsymbol{\theta})}{\partial \boldsymbol{\theta}} \right]^T p_R(\mathbf{r}; \boldsymbol{\theta}) d\mathbf{r}. \quad (16)$$

Compared to Theorem 2.1, which showed an exact match of the GFIM with the FIM, Theorem 2.3 (proved in Appendix B) includes an error term, introduced by trimming the support of the distribution  $p_R(\mathbf{r}; \boldsymbol{\theta})$  from  $\Upsilon$  to  $\hat{\Upsilon}$ .

To further characterize this truncation error, we assume in the rest of this section that the measurement distribution has a bounded score vector.

**Assumption 2.5 (Bounded True Score Vector):**

$$\left\| \frac{\partial \mathbf{L}_R(\boldsymbol{\theta})}{\partial \boldsymbol{\theta}} \right\| = \frac{1}{p_R(\mathbf{r}; \boldsymbol{\theta})} \left\| \frac{\partial p_R(\mathbf{r}; \boldsymbol{\theta})}{\partial \boldsymbol{\theta}} \right\| \leq C_R(\boldsymbol{\theta})$$

$$\forall \boldsymbol{\theta} \in \Theta, \forall \mathbf{r} \in \Upsilon.$$

Note that this assumption is a little more restrictive version of Assumption A.2. We then have the following.

**Corollary 3.1:**

$$\hat{\mathbf{F}}_G(\boldsymbol{\theta}) \xrightarrow{\epsilon_r \rightarrow 0} \mathbf{F}_R(\boldsymbol{\theta})$$

*Proof:* Using Assumption 2.5,

$$\frac{\partial \mathbf{L}_R(\mathbf{r}; \boldsymbol{\theta})}{\partial \boldsymbol{\theta}} \left[ \frac{\partial \mathbf{L}_R(\mathbf{r}; \boldsymbol{\theta})}{\partial \boldsymbol{\theta}} \right]^T \prec C_R^2(\boldsymbol{\theta}) \mathbf{I}$$

and therefore by (16)  $\epsilon_t(\boldsymbol{\theta}) \prec C_R^2(\boldsymbol{\theta}) \mathbf{I} \int_{\Upsilon \setminus \hat{\Upsilon}} p_R(\mathbf{r}; \boldsymbol{\theta}) d\mathbf{r}$ .

Applying Assumption A.8 yields  $\epsilon_t(\boldsymbol{\theta}) \prec \epsilon_r C_R^2(\boldsymbol{\theta}) \mathbf{I}$ . ■

It follows that if Assumptions 2.4 and 2.5 holds then the trimmed GFIM converges to the FIM almost surely as  $\epsilon_r \rightarrow 0$ .

**Corollary 3.2:**

$$\overline{\text{GCRB}}_G(\boldsymbol{\theta}) \xrightarrow[\epsilon_r \rightarrow 0]{m \rightarrow \infty} \text{CRB}_R(\boldsymbol{\theta}) \quad \text{a.s.}$$

*Proof:* By the strong Law of Large numbers  $\lim_{m \rightarrow \infty} \overline{\mathbf{F}}_G(\boldsymbol{\theta}) = \hat{\mathbf{F}}_G(\boldsymbol{\theta})$  a.s. Combining this with Corollary 3.1 and inverting yields the result. ■

It follows that if Assumptions 2.4 and 2.5 hold then the eGCRB converges to the CRB almost surely as  $m \rightarrow \infty$  and  $\epsilon_r \rightarrow 0$ . Recalling that using the proposed adaptive trimming criterion we have that  $\epsilon_r \rightarrow 0$  as  $|\mathcal{D}| \rightarrow \infty$ , it follows that, subject to Assumptions 2.4 and 2.5 with sufficient training data and sufficient sampling from the generator, the eGCRB will approximate the CRB arbitrarily well.

### III. NORMALIZING FLOWS

We use a normalizing flow [13], [14], a class of (invertible) neural networks to obtain  $\mathbf{G}$  and  $\nu$ . Here, we give a brief overview of the normalizing flows utilized in this paper. Specifically, we will present conditional normalizing flow (CNF) where the normalizing flow is conditioned on the input parameter  $\boldsymbol{\theta}$ . A CNF transforms a random variable with a known distribution (typically Normal) through a sequence of differentiable, invertible mappings. Formally, let  $\mathbf{z}_1, \dots, \mathbf{z}_{n_l}$  be a sequence of random variables that are related as  $\mathbf{z}_i = \mathbf{G}_i(\mathbf{z}_{i-1}; \boldsymbol{\theta})$ , where for each  $\boldsymbol{\theta} \in \Theta$  the function  $\mathbf{G}_i(\cdot; \boldsymbol{\theta}) : \mathbb{R}^d \rightarrow \mathbb{R}^d$  is a differentiable and

bijjective,  $n_l$  is the number of flow layers, and  $\mathbf{z} = \mathbf{z}_0$  a random variable with a known and tractable probability density function  $p_{\mathbf{z}} : \mathbb{R}^d \rightarrow \mathbb{R}$ . Then defining  $\Gamma \triangleq G(\mathbf{z}_0; \boldsymbol{\theta}) = G_{n_l} \circ G_{n_l-1} \circ \dots \circ G_1(\mathbf{z}_0; \boldsymbol{\theta})$  as a composition of the  $G_i$ , the transformation of a random variables formula says that the probability density function for  $\Gamma$  is

$$\begin{aligned} p_{\Gamma}(\boldsymbol{\gamma}; \boldsymbol{\theta}) &= p_{\mathbf{z}}(\nu(\boldsymbol{\gamma}; \boldsymbol{\theta})) |\det \mathbf{J}_{\nu}(\boldsymbol{\gamma}; \boldsymbol{\theta})|, \\ &= p_{\mathbf{z}}(\nu(\boldsymbol{\gamma}; \boldsymbol{\theta})) \prod_{j=1}^{n_l} |\det \mathbf{J}_j(\mathbf{z}_j; \boldsymbol{\theta})|, \end{aligned} \quad (17)$$

where for each fixed  $\boldsymbol{\theta}$ ,  $\nu = \nu_1 \circ \nu_2 \circ \dots \circ \nu_{n_l}$  and  $\nu_i$  are the inverses of  $G$  and of  $G_i$  with respect to their first argument and  $\mathbf{J}_j(\mathbf{z}_{j-1}; \boldsymbol{\theta}) = \frac{\partial \nu_j(\mathbf{z}_{j-1}; \boldsymbol{\theta})}{\partial \mathbf{z}_{j-1}}$  is the Jacobian of the  $j^{\text{th}}$  transformation  $\nu_j$  with respect to its input  $\mathbf{z}_{j-1}$ . We denote the value of the  $j^{\text{th}}$  intermediate flow as  $\mathbf{z}_j = G_j \circ \dots \circ G_1(\mathbf{z}_0; \boldsymbol{\theta}) = \nu_{j+1} \circ \dots \circ \nu_{n_l}(\boldsymbol{\gamma}; \boldsymbol{\theta})$  and  $\boldsymbol{\gamma} = \mathbf{z}_{n_l}$ .

**Density Learning** A CNF can be directly used for density learning by finding parameters that minimize the negative log-likelihood (NLL) over a set of samples where the likelihood is given by (17). Given a dataset  $\mathcal{D}$  (see Problem 1) and the transformations  $G_1, \dots, G_{n_l}$  parameterized by  $\Omega = (\omega_1, \dots, \omega_{n_l})$  respectively, the negative log-likelihood is given by:

$$\begin{aligned} L(\Omega) &= - \sum_i \log(p_{\mathbf{z}}(\nu(\mathbf{r}_i; \boldsymbol{\theta}_i | \Omega))) \\ &\quad - \sum_i \sum_j \log(|\det \mathbf{J}_j(\mathbf{u}_{ij}; \boldsymbol{\theta}_i | \Omega)|). \end{aligned} \quad (18)$$

where  $\mathbf{u}_{ij} = \nu_{j+1} \circ \dots \circ \nu_{n_l}(\mathbf{r}_i; \boldsymbol{\theta})$  denotes the intermediate flow of the  $i^{\text{th}}$  sample and the  $j^{\text{th}}$  layer. Note that the first term is the negative log-likelihood of the sample under the base measure (latent distribution) and the second term is a differential volume correction, which accounts for the change of differential volume induced by the transformations.

We use a CNF based on the Glow [10] architecture, which includes the following flow steps: Activation Normalization, Affine Coupling, and so-called 1x1 convolution (an invertible matrix operation). These flow steps transport the base distribution into the target distribution. However, we take the SRFlow approach [26] for the insertion of the conditioning parameter using the Affine Inject flow step that modifies the transformation according to the conditional parameter  $\boldsymbol{\theta}$ . Furthermore, in some cases (e.g., in the non-Gaussian measurement example of Sec. IV-A.2), a more complex modification of the base distribution is required, and this is achieved by replacing the Affine Coupling with a Cubic Spline Coupling flow [27]. The flow steps mentioned above are detailed in Appendix E.

#### IV. MEASUREMENTS MODEL EXAMPLES

First, we present two simple examples in which we can compute both the CRB and GCRB analytically and obtain an optimal generator. Note that by "optimal" we mean

that the generator distribution  $p_{\Gamma}(\mathbf{r}; \boldsymbol{\theta})$  is identical to the data distribution  $p_{\mathbf{R}}(\mathbf{r}; \boldsymbol{\theta})$ , meaning that Assumption 2.4 holds. Then in the second part, we present a real-world measurement model of cameras, which will be used to demonstrate some of the benefits of the GCRB.

##### A. Simple Measurement Models

1) *Linear Gaussian*: Let

$$\mathbf{R}(\boldsymbol{\theta}) = \mathbf{A}\boldsymbol{\theta} + \mathbf{v}, \quad (19)$$

where matrix  $\mathbf{A} \in \mathbb{R}^{d \times k}$  with  $d > k$  and  $\mathbf{v} \sim \mathcal{N}(0, \mathbf{C}_{vv})$  is an additive zero-mean Gaussian noise with positive-definite covariance  $\mathbf{C}_{vv} \in \mathbb{R}^{d \times d}$ . Then the measurement is distributed as  $\mathbf{R}(\boldsymbol{\theta}) \sim \mathcal{N}(\mathbf{A}\boldsymbol{\theta}, \mathbf{C}_{vv})$ , which provides a complete description of the measurement channel. The CRB for  $\boldsymbol{\theta}$  coincides with the expression for the covariance of the linear unbiased minimum variance estimator and is given by [2]:

$$\text{CRB}_R(\boldsymbol{\theta}) = [\mathbf{A}^T \mathbf{C}_{vv}^{-1} \mathbf{A}]^{-1}.$$

Now we present an optimal generator for this example. Let  $G(\mathbf{z}; \boldsymbol{\theta}) = \mathbf{A}\boldsymbol{\theta} + \mathbf{L}\mathbf{z}$ , where  $\mathbf{z} \sim \mathcal{N}(0, \mathbf{I})$  and  $\mathbf{L}$  is a square root (e.g., the Cholesky) factor of  $\mathbf{C}_{vv}$ , that is,  $\mathbf{L}\mathbf{L}^T = \mathbf{C}_{vv}$ . Then, as easily verified,  $G$  is an optimal generator, because for any  $\boldsymbol{\theta}$  the distribution  $G(\mathbf{z}) \sim \mathcal{N}(\mathbf{A}\boldsymbol{\theta}, \mathbf{C}_{vv})$  coincides with that of  $\mathbf{R}(\boldsymbol{\theta})$ . The inverse function of  $G$ , the normalizing flow, is  $\nu(\boldsymbol{\gamma}; \boldsymbol{\theta}) = \mathbf{L}^{-1}(\boldsymbol{\gamma} - \mathbf{A}\boldsymbol{\theta})$ . To compute the score vector, we need the derivatives of the base distribution and of the normalizing flow:

$$\begin{aligned} \frac{\partial \log p_{\mathbf{z}}(\mathbf{z})}{\partial \mathbf{z}} &= -\mathbf{z} \\ \left. \frac{\partial \nu(\boldsymbol{\gamma}; \boldsymbol{\theta})^T}{\partial \boldsymbol{\theta}} \right|_{\boldsymbol{\gamma}=G(\mathbf{z}; \boldsymbol{\theta})} &= \mathbf{L}^{-1} \mathbf{A} \\ \mathbf{J}_{\nu}^{-1}(\boldsymbol{\gamma}; \boldsymbol{\theta}) &= \mathbf{L} \end{aligned} \quad (20)$$

Then, substituting Equations (20) into (6), we compute the score vector corresponding to the optimal normalizing flow:

$$\mathbf{s}_{\boldsymbol{\theta}}(\mathbf{z}) = -\mathbf{A}^T (\mathbf{L}^{-1})^T \mathbf{z},$$

and the GFIM corresponding to the optimal generator obtained using (8) is

$$\mathbf{F}_G(\boldsymbol{\theta}) = \mathbb{E}_{\mathbf{z}} [\mathbf{A}^T (\mathbf{L}^{-1})^T \mathbf{z} \mathbf{z}^T \mathbf{L}^{-1} \mathbf{A}].$$

Simplifying and taking the inverse results in  $\mathbf{F}_G(\boldsymbol{\theta})^{-1} = \text{GCRB}_G(\boldsymbol{\theta}) = \text{CRB}_R(\boldsymbol{\theta})$ . This confirms, that as expected, an optimal generator will yield the same CRB on the parameter vector  $\boldsymbol{\theta}$  as the correct distribution.

2) *Scale Non-Gaussian*: Here, we show a scale model with non-Gaussian distribution. Consider the data model

$$r = y\theta, \quad (21)$$

where  $\theta \in \mathbb{R}^+$  is the desired parameter and  $y$  is a random variable with the PDF

$$p_Y(y) = \frac{1}{\sqrt{2\pi}\sigma^2} 3y^2 \cdot \exp\left(-\frac{1}{2\sigma^2} y^6\right). \quad (22)$$

Then, as shown in Appendix F, the FIM of  $\theta$  is  $F_R(\theta) = 18\theta^{-2}$  and  $\text{CRB}_R(\theta) = \frac{\theta^2}{18}$ . We show in Appendix F.1 that  $\Gamma(\theta) = G(z; \theta) = \theta z^{\frac{1}{3}}$  is an optimal generator, that is  $\Gamma(\theta) \sim p_{R;\theta}(r; \theta)$ . The inverse function of the optimal generator is the normalizing flow  $\nu(\gamma; \theta) = (\frac{\gamma}{\theta})^3$ . To compute the score vector we need the derivative and Jacobian of the normalizing flow:

$$\begin{aligned} \left. \frac{\partial \nu(\gamma; \theta)}{\partial \theta} \right|_{\gamma=G(z; \theta)} &= -\frac{3z}{\theta} \\ \mathbf{J}_\nu(\gamma; \theta) &= 3\frac{\gamma^2}{\theta^3} \\ \left. \frac{\partial \mathbf{J}_\nu(\gamma; \theta)}{\partial \theta} \right|_{\gamma=G(z; \theta)} &= -9\frac{\gamma^2}{\theta^4} \\ \mathbf{J}_\nu^{-1}(\gamma; \theta) \left. \frac{\partial \mathbf{J}_\nu(\gamma; \theta)}{\partial \theta} \right|_{\gamma=G(z; \theta)} &= -\frac{3}{\theta} \end{aligned} \quad (23)$$

Then using (23) we compute the score vector (6) of the optimal generator and normalizing flow, which yields

$$\mathbf{s}_\theta(z) = -\theta^{-1} 3(1 - z^2).$$

Finally, the FIM of the optimal generator obtained using (8) is

$$F_G(\theta) = \mathbb{E}_z \left[ (\theta^{-1} 3(1 - z^2))^2 \right] = 18\theta^{-2}, \quad (24)$$

where the last equality follows by the Gaussian moment property. Hence  $\text{GCRB}_G(\theta) = \text{CRB}_R(\theta)$ . This example demonstrates that an optimal generator yields the correct CRB on the parameter in a non-Gaussian case.

## B. Image Processing

We consider two classical image processing problems, however with a real-world learned measurement model of 4-channel (RGGB) color image sensors using NoiseFlow [6], a normalizing flow that models camera noise. Using this learned model, we obtain the GCRB for these two problems.

**1) Image Denoising:** Image denoising is a well-known problem in signal processing, however modeling camera noise is a challenging task [28], [29]. Due to the difficulty of noise modeling, it is impossible to compute an analytical lower bound on denoising performance on a realistic model.

Formally the denoising problem is defined as follows. Denoting by  $\mathbf{H}$  a clean 4-channel (RGGB) image patch and by  $\mathbf{V}$  the camera noise, the noisy image tensor is defined as

$$\tilde{\mathbf{H}} = \mathbf{H} + \mathbf{V}. \quad (25)$$

Our goal is to provide a lower bound on the performance of any unbiased estimator that estimates the clean image  $\mathbf{H}$  from the noisy image  $\tilde{\mathbf{H}}$ . Under this model, denoting by  $\text{Vec}(\mathbf{T})$  the vectorization of tensor  $\mathbf{T}$ ,  $\mathbf{R} = \text{Vec}(\tilde{\mathbf{H}})$  is the measurement vector and  $\theta = \text{Vec}(\mathbf{H})$  is the parameter vector.

**2) Edge Detection:** Another interesting image processing task is edge detection. Here we describe the edge model used in this work. Consider a  $c$ -channel image of width  $h$  pixels, and let  $\mathbf{H}_{ijc} = f_{ijc}(\theta_p)$  be a vertical edge function that maps a continuous-valued edge position parameter  $\theta_p \in [0, h-1]$ , to the image color values at horizontal and vertical pixel position  $i, j$  and image channel  $c$ . The edge function is specified in terms of a horizontal color scaling function  $s_i(\theta_p) : [0, h-1] \rightarrow [0, 1]$  as

$$f_{ijc}(\theta_p) = (p_c^h - p_c^l) \cdot s_i(\theta_p) + p_c^l,$$

where  $p^h$  and  $p^l$  are the vectors of RGGB pixel values for high and low intensities, respectively. The color scaling function is defined as

$$s_i(\theta_p) = \phi\left(\frac{\theta_p - i}{e}\right),$$

where  $e$  is the edge width, and  $\phi$  is the Sigmoid function  $\phi(x) = \frac{1}{1+\exp(-x)}$ . Images with edges of different position and width following the model above are shown in Fig. 2.

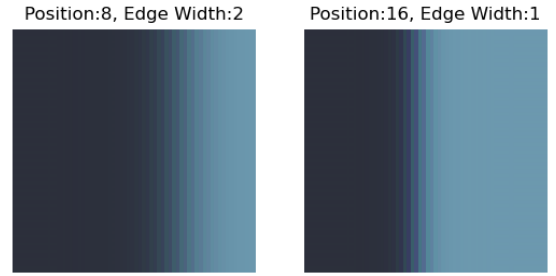


Fig. 2: Edges in a clean image

In this example we want to estimate the edge position  $\theta_p$  from a noisy image  $\tilde{\mathbf{H}}$ . We compare the GCRB with NoiseFlow to the CRB derived for two well-known analytical Gaussian noise models: (i) i.i.d, or white Gaussian noise (WGN); and (ii) independent noise with image-dependent intensity - the so-called noise level function (NLF) noise model. The WGN model ( $\mathbf{V}_{ijc} \sim \mathcal{N}(0, \sigma^2)$ ) with i.i.d noise in each channel of each pixel and variance  $\sigma^2$  has CRB

$$\text{CRB}_W(\theta_p) = \frac{\sigma^2 e^2 \left( \sum_i s_i(\theta_p)^2 (1 - s_i(\theta_p))^2 \right)^{-1}}{h \|\mathbf{p}^h - \mathbf{p}^l\|_2^2}. \quad (26)$$

The NLF model with  $\mathbf{V}_{ijc} \sim \mathcal{N}(0, \alpha^2 f_{ijc}(\theta_p) + \delta^2)$ , where  $\alpha$  and  $\delta$  are the noise parameters, has CRB

$$\text{CRB}_{\text{NLF}}(\theta_p) = \left( \sum_{i,j,c} \frac{\alpha^2 (1 + 2f_{ijc}(\theta_p)) + 2\delta^2}{2(\alpha^2 f_{ijc}(\theta_p) + \delta^2)^2} \left[ \frac{\partial f_{ijc}(\theta_p)}{\partial \theta_p} \right]^2 \right)^{-1}, \quad (27a)$$

$$\left[ \frac{\partial f_{ijc}(\theta_p)}{\partial \theta_p} \right] = \frac{(p_c^h - p_c^l)}{e} s_i(\theta_p) (1 - s_i(\theta_p)). \quad (27b)$$

A detailed calculation of CRB's is given in Appendix G.

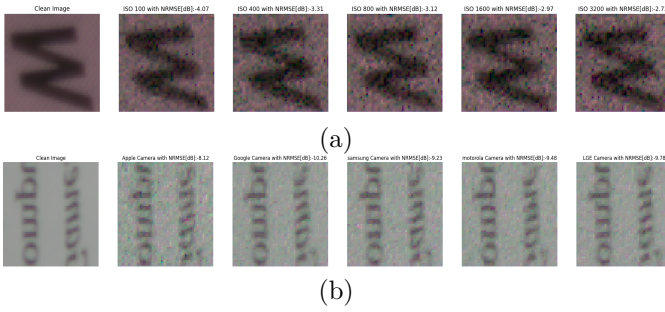


Fig. 3: NoiseFlow output: clean and noisy images. (a) Different ISO levels, for Camera Type=zero (Apple). (b) Different cameras at ISO level 100.

3) *Camera Noise Model*: Several recent works [6], [30] have used a data-driven approach to model camera noise. We use NoiseFlow [6] to model a realistic camera noise  $\mathbf{V} \sim p_{\mathbf{V}}(\mathbf{v}; \mathbf{H})$  and similarly to model the noisy image  $\tilde{\mathbf{H}} \sim p_{\tilde{\mathbf{H}}}(\tilde{\mathbf{h}}; \mathbf{H})$ . To obtain a noisy image flow, we cascade to NoiseFlow an AdditiveNoise Flow layer corresponding to (25), defined as

$$\mathbf{z}_{n+1} = \mathbf{H} + \mathbf{z}_n. \quad (28)$$

The inverse of (28) is given by  $\mathbf{z}_n = \mathbf{z}_{n+1} - \mathbf{H}$  and the log-determinant term is zero. Note that the ability to incorporate a signal model into the normalizing flow is a well-known advantage, which has also been exploited in NoiseFlow [6].

NoiseFlow is trained using the Smartphone Image Denoising Dataset (SIDD) [31]. The SIDD dataset consists of 150 noisy and corresponding clean images captured in ten different scenes, with five smartphone cameras of different brands, under several lighting conditions and ISO (sensitivity) levels. Specifically, NoiseFlow is trained on  $h_p = 32 \times w_p = 32$  pixel RGGB patches of clean image and noise  $\mathbf{H}, \mathbf{V} \in \mathbb{R}^{h_p \times w_p \times 4}$ .

Fig. 3 shows examples of clean images and the corresponding noisy images generated by NoiseFlow at different ISO levels and for different camera devices. They illustrate the strong ISO, device, and image dependence of the noise, which cannot be captured by an analytical model, thus precluding traditional calculation of estimation bounds. Instead, using this learned model, we obtain the GCRB for the two problems of image denoising and edge position detection.

## V. EXPERIMENTAL RESULTS

This section presents a set of numerical experiments for assessing, analyzing, and demonstrating the GCRB. In the first set of experiments, we determine the quality of the approximation provided by the GCRB by evaluating the eGCRB on the examples in Section IV-A and comparing to the true, analytically derived CRB. In the second set of experiments, we study, for the linear estimation problem, the approximation error of the eGCRB due to imperfect training, and due to the use of the sample mean to estimate the expected value. For the last two experiments, we

present the usage of GCRB on the real-world examples of image denoising and edge detection in a device-dependent noise. Unless stated otherwise, we evaluate the eGCRB using  $m = 64K$  generated samples in the sample mean in all experiments. In all experiments, the computation is done using Nvidia 1080Ti GPU running white PyTorch [17].

### A. Approximation Quality

We evaluate the accuracy of the approximation to the CRB provided by the GCRB using two kinds of normalizing flows: (i) the optimal flow, which satisfies the condition of perfectly matched distribution (11); and (ii) a standard/learned normalizing flow (see Sec. III), which is trained using the dataset  $\mathcal{D}$ .

Unless stated otherwise, we use the following parameters in the training process of all experiments. For training a normalizing flow, we use the conditional negative log-likelihood (NLL) of the training set (18) as the loss function. We train each normalizing flow using a dataset of 200k samples for 90 epochs with batch size 64. We use the Adam optimizer [32] with learning rate  $1e-4$  and parameters  $\beta_1 = 0.9$  and  $\beta_2 = 0.999$ . At the end of training, we obtain the learned normalizing flow  $\nu$  and its inverse (the generator)  $G$  and evaluate the eGCRB at several  $\theta$  values using Algorithm 1. The latent variable is chosen to be  $\mathbf{z} \sim \mathcal{N}(0, \mathbf{I})$  in all examples. We begin by showing the approximation quality in the two examples presented in Sec. IV-A, and then investigate the source of approximation error.

**Linear Example** For the linear model (19) we use  $d = 8$ ,  $\sigma_v = 2.0$  and  $k = 2$ . Hence  $\theta \in \mathbb{R}^2$  and  $R(\theta_i) \in \mathbb{R}^8$ . We generate the training dataset  $\mathcal{D}$  in the following manner. First, we generate matrices  $\mathbf{A}$  and  $\mathbf{L}$  using a standard normal distribution, and use the same two matrices to generate all the samples in  $\mathcal{D}$ . For each sample  $(\theta_i, R(\theta_i)) \in \mathcal{D}$ , the parameter vector  $\theta_i \in \mathbb{R}^2$  is drawn i.i.d from a uniform distribution  $\theta_i \sim U[-2, 2]^2$ ,  $\mathbf{v}_i \in \mathbb{R}^8$  is drawn i.i.d Normal  $\mathbf{v}_i \sim \mathcal{N}(0, \mathbf{C}_{vv})$  with  $\mathbf{C}_{vv} = \mathbf{L}\mathbf{L}^T$ , and  $R(\theta_i) \in \mathbb{R}^8$  is computed using (19). Using this dataset, we train a normalizing flow with the architecture shown in Appendix H.3, obtaining  $\nu$  and  $G$ .

We chose an architecture with invertible  $1 \times 1$  convolution and affine inject since it can represent an optimal generator and satisfies the  $G \in C^2$  condition.

Then, for each value of  $\theta$  of interest, we use the trained generator to generate samples of the score vector, and compute the eGFIM using (9), which yields, upon inversion, the eGCRB. For comparison, we repeat the generation of the score vector using the optimal normalizing flow and generator instead of the learned flow and generator.

In Fig. 4 we display the traces of the two eGCRBs, as well as that of the analytical CRB, for  $\theta = (\xi, \xi)^T$ , with  $\xi$  on a uniform grid on the interval  $[-2, 2]$ . Figure 4 shows that a learned normalizing flow can estimate the true CRB to a good accuracy. Because (as we verified) the specific



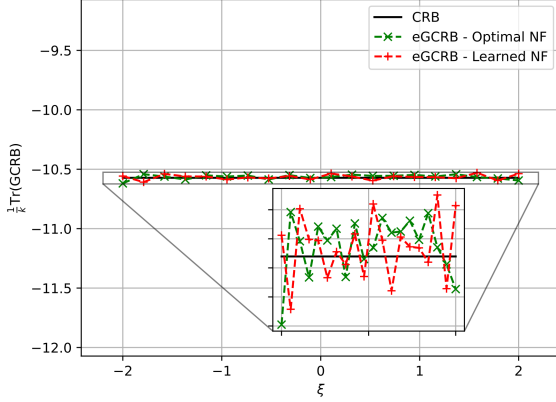


Fig. 4: Trace of CRB and eGCRB for the linear measurement model (19).

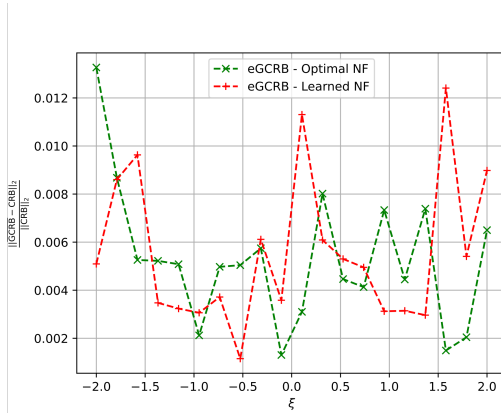


Fig. 5: Relative error between the eGCRB and CRB for the linear measurement model (19) at  $\theta = (\xi, \xi)^T$  as a function of  $\xi$ . The eGCRBs obtained using an optimal and learned flow are compared.

parameter values  $\theta$  shown in Fig. 4 are not present in the training set, this also demonstrates that the GCRB works well for unseen examples. As expected, on the average the eGCRB using the optimal flow has slightly better accuracy than the one using the learned flow, because the former only suffers from the finite sampling error in estimating the GFIM using an empirical mean, whereas the latter is also subject to the imperfectly learned flow model. The relative error (13) of the eGCRB is displayed in Figure 5 for both learned and optimal flows, showing that both have comparable accuracy, of within  $\approx 0.5\%$  from the true CRB.

**Scale Example** In this example we generate the training dataset  $\mathcal{D}$  in the following manner. For each sample  $(\theta_i, R(\theta_i)) \in \mathcal{D}$ , the parameter  $\theta_i$  is drawn i.i.d from a uniform distribution  $\theta_i \sim U[3, 6]$ ,  $y$  is drawn i.i.d  $y \sim p_Y$ , where  $p_Y$  is given by (22) and  $R(\theta_i) = y\theta_i$ , per (21). To produce a vector input to the normalizing flow, as needed for the application of affine coupling, we define a vector measurement of length 2, composed of two i.i.d samples

with the same parameter  $\theta_i$ .<sup>1</sup> Note that since this vector measurement corresponds to two i.i.d measurements, by the additivity property of the FIM, this only scales the resulting GFIM by a factor of 2. Using this dataset  $\mathcal{D}$  we train a normalizing flow with the architecture shown in Appendix H. We chose an architecture with cubic-spline and affine inject since it can locally represent an optimal generator and satisfies the  $G \in C^2$  condition.

Then, we follow the same procedure as for the linear measurement model to produce the eGCRB using both the learned flow and the optimal flow. The two eGCRB values and the true CRB are compared in Fig. 6.

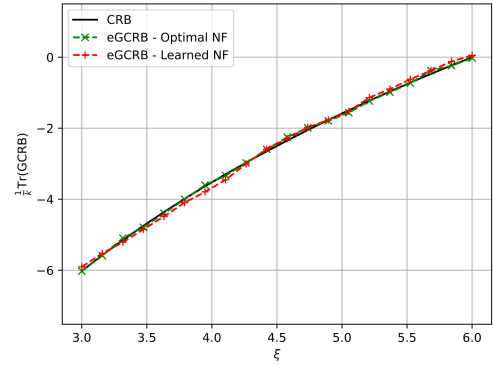


Fig. 6: Analytical CRB and eGCRBs for the scale model (21),(22), using the optimal flow and a learned flow.

Figure 6 demonstrates that a learned normalizing flow can estimate the true CRB in the non-Gaussian case, with accuracy comparable to that of the optimal flow. Similar to the linear example, because (as we verified) the parameter values  $\theta$  used to plot Fig 6 are not present in the training set, this again demonstrates the interpolation capability of the GCRB to provide a good approximation for unseen examples.

To summarize, Fig. 6 and Fig. 4 demonstrate Theorem 2.1, which states that given a well-trained generative model (11), the GCRB matches the CRB. Both figures show random deviations of the eGCRB from the CRB due to two reasons: (i) imperfectly trained generative model; and (ii) a finite number of samples used to calculate empirical mean, as stated in Theorem 2.2. Moreover, the eGCRBs in Fig. 4 and Fig. 6 are evaluated at points that are not present in the training set, which shows the ability of GCRB to interpolate the CRB values to those points.

## B. Error Analysis

Here, we study further the approximation error due to the empirical mean and imperfect training. We use two metrics for the error:

$$\text{MRE} = \max_{\theta \in \Theta_T} \text{RE}(\theta),$$

<sup>1</sup>We use this form, rather than padding with an unrelated standard normal random variable, to mitigate issues of exploding condition number [21].

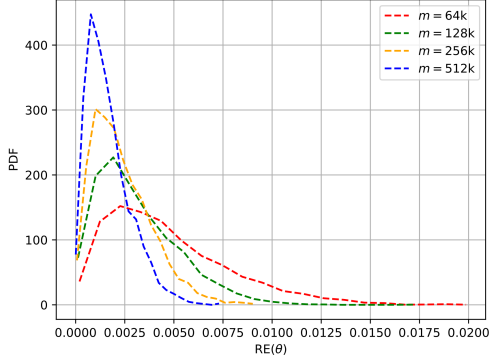


Fig. 7: Histogram of  $\text{RE}(\theta)$  for the linear example using different number of samples  $m \in \{64k, 128k, 256k, 512k\}$ .

$$\overline{\text{MRE}} = \frac{1}{|\Theta_T|} \sum_{\theta \in \Theta_T} \text{RE}(\theta),$$

where MRE and  $\overline{\text{MRE}}$  are the maximal and mean relative norm error, respectively,  $\Theta_T \subset \Theta$  is the set of  $\theta$  value used in the validation process, and  $|\Theta_T|$  is the cardinality of the set  $\Theta_T$ . In this experiment, we verify Theorem 2.2 using the linear optimal model with the same parameters as above and evaluate eGCRB with different number of samples  $m \in \{64K, 128K, 256K, 512K\}$ . We repeat the evaluation for each  $m$  2000 times and present the histogram of the relative norm error  $\text{RE}(\theta)$  in Figure 7. In all the trials we use the same parameter vector  $\theta = (0.2, 0.2)^T$ .

We see in Fig. 7 the effect of different  $m$  values on the distribution of the relative error. This confirms, that as predicted by Theorem 2.2, for the optimal generator, we can make the eGCRB error arbitrary small by increasing the number of samples  $m$  to calculate the eGFIM (9). This addresses the error due to sampling assuming a well-trained normalizing flow.

In the next experiment, we address the error due to imperfect training. To focus on this aspect, we set  $m = 512k$ , so that the error due to the empirical mean is negligible. We train a normalizing flow on the linear problem using various dataset sizes, and report the maximal and mean relative error. To train a normalizing flow with a small dataset size, we adjust the number of epochs to have a constant number of gradient updates, by setting the number of epochs to  $\lceil 90 \frac{200e^3}{|\mathcal{D}|} \rceil$  where  $|\mathcal{D}|$  is the size of the dataset and  $\lceil x \rceil$  denotes the ceiling of  $x$ . In Fig. 8 we present the MRE for different dataset size and validation parameter set  $\Theta$  consisting of 20 points  $\theta = (\xi, \xi)^T$  with  $\xi \in [-2, 2]$  uniformly spaced.

Fig. 8 shows relative error decreasing with increasing training set size, highlighting the importance of training to obtain a well-trained generative model. However, increasing the dataset size beyond some point (in this case, above 50K samples) doesn't improve the results. To interpret this saturation effect, recall that the normalizing flow used in this problem can represent the optimal generator, hence

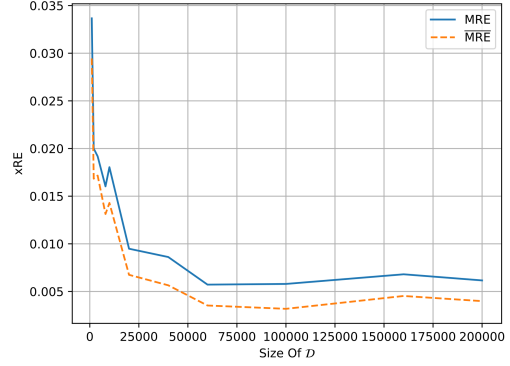


Fig. 8: MRE and  $\overline{\text{MRE}}$  for the linear measurement model example vs. training dataset size.

a limitation in representation capacity by the normalizing flow is not the culprit. Instead, comparison with Fig. 7 suggests that for  $|\mathcal{D}| > 5 \cdot 10^4$  the error in this learned generator experiment is dominated by the empirical mean error - with similar values as when using an optimal generator.

### C. Image Denoising

Here, we study the GCRB for the Image denoising problem, using the NoiseFlow [6] to model the image noise. Noise Flow is composed of affine coupling, invertible  $1 \times 1$  convolution, gain layer (which is a constant affine transformation), and signal-dependent layer (which is similar to affine inject with a predefined function). First, we replace the ReLU activation function in the original NoiseFlow to Sigmoid Linear Unit (SiLU) [33], to satisfy the requirement that  $G \in C^2$ . Then, we train the modified Noise-Flow from scratch using the authors' original code [34]. We obtained NNL of  $-3.528$  which is a similar to that in the original NoiseFlow. Then, we add to NoiseFlow an AdditiveNoise layer (see Section IV-B.3), which provides a noisy image. We generate all the required derivatives using the PyTorch built-in symbolic differentiation invoked using standard PyTorch commands, and utilize our eGCRB computing formulas to provide an approximation to the CRB. We compute the eGCRB using (9) with  $m = 64k$ .

Note that for image visualization purposes only, we render RGG images through a color processing pipeline into sRGB color space. Moreover, to visualize the eGCRB, we extract the diagonal of the eGCRB matrix and present the lower bound for each channels (R, G, G, B) separately. In all experiments we use an image size of  $h = w = 32$  and batch-size 32.

We present the bounds on the denoising performance in normalized form, by computing the following metrics

$$\text{NPRMSE}_{ijc} \triangleq \frac{\sqrt{g(\text{diag}(\overline{\text{GCRB}}))_{ijc}}}{I_{ijc}}, \quad (30a)$$

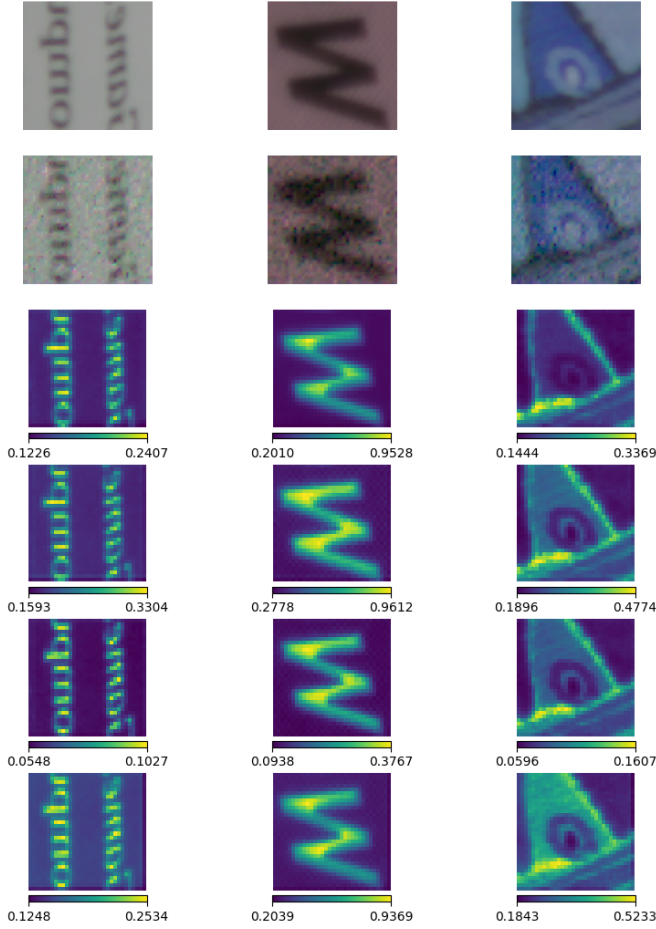


Fig. 9: GCRB for the denoising problem on three scenes (one per column). 1st and 2nd rows: clean and noisy image, respectively. Last four last rows: NPMSE of the R, G, G, B channels. Camera type zero (Apple).

$$\text{NRMSE} \triangleq \sqrt{\frac{1}{hwc} \sum_{i,j,c} \text{NPMSE}_{ijc}^2}. \quad (30b)$$

The  $\text{NPRMSE}_{ijc}$  is the normalized per pixel bound on the error standard deviation error,  $\text{diag}(\mathbf{A})$  denotes the diagonal vector of matrix  $\mathbf{A}$ ,  $g() : \mathbb{R}^{h \cdot w \cdot c} \rightarrow \mathbb{R}^{h \times w \times c}$  is the reshaping of vector to RGB image, and  $i, j, c$  are the vertical, horizontal and channel indices, respectively. In turn, NRMSE is the square of the per pixel NPRMSE, averaged over the entire image followed by a square root.

Note that the metrics in (30) take into account only the diagonal elements of the eGCRB. However, both the eGFIM and the eGCRB have off-diagonal elements thanks to the ability of NoiseFlow to generate correlated noise that models the sensor. This correlation is evident in the non-zero off-diagonals in the eGFIM, and affects the diagonal elements of the eGCRB.

In this study, we perform several experiments. First, we present several visual examples in Fig. 9. The top row shows three clean images to which we refer, from left to right, as scene one, two, and three. The second row shows the corresponding noisy versions for Camera 0 (Apple) at ISO = 100. The next four rows display (as images

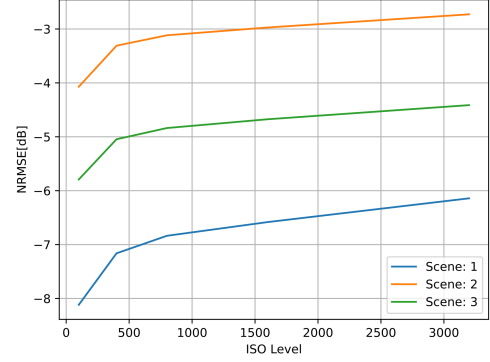


Fig. 10: Lower bound on the denoising error vs. ISO levels. The lines correspond to Scene 1 - Scene 3 on the first row of Fig. 9.

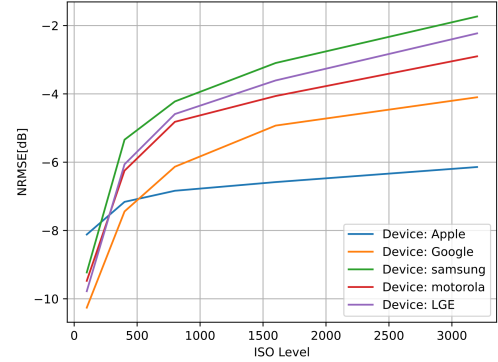


Fig. 11: Lower bound on the denoising error for Scene 1 of Fig. 9 vs. ISO level for five different devices.

color-coded by magnitude) the normalized lower bound on the denoising error standard deviation for each pixel (i.e., the  $\text{NPRMSE}_{ijc}$ ): one row for each of the four channels  $c = 1, 2, 3, 4$ . We observe that pixels with different colors have distinct lower bounds, showing the effect of the Signal Depend Layer in NoiseFlow [6]. An analogous behavior is seen in the NFL model which scales the noise by the clean image values. It is also seen that brighter pixels have a better (smaller) normalized lower bound than darker ones.

Next, in Fig.10 we plot the normalized lower bound on the denoising performance using Device=0 (Apple) on the same three scenes as in Fig. 9. It is seen that a lower ISO level allows better denoising than a higher one, and that different scenes have different denoising lower bounds. For an insight as to whether the difference is due to color level, scene structure, or both, we refer to Fig. 3. It reveals that the noise level increases with ISO level, and is relatively higher in darker (lower color level) areas. The first property clearly accounts for the increase in the bound vs. ISO level seen in Fig.10, whereas the second property explains the relative ranking of the bounds for the three scenes, with increasing normalized bound for darker images.

Figure 11 shows, for Scene 1, the effect of different

measurement devices. The relative ranking in terms of the denoising bound cannot be inferred from the visual impression of the noise for the different devices in Fig. 3. However, it remains the same for Scene 2 and Scene 3, showing consistency of the bounds for each device. These results demonstrate a unique advantage of the GCRB, which can provide a bound specific to a measurement device.

#### D. Edge Detection

We use the same parameters as used in the image denoising problem. First, in Fig. 12, we present a lower bound on edge position estimate vs. the position of the edge in the image, for several different edge widths, using Device=0 (Apple) and ISO level 100.

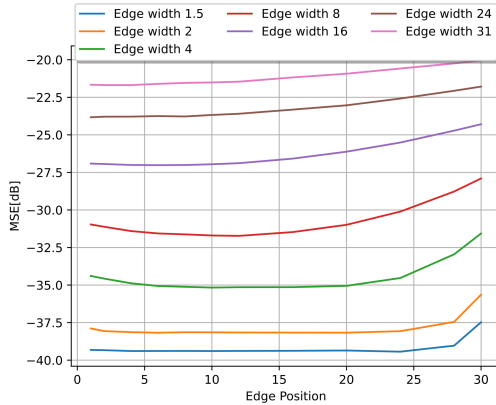


Fig. 12: Lower bound on edge position with different edge widths using Device=0 (Apple) at ISO 100.

Fig. 12 reveals different behavior of the edge localization bound for different edge widths. First, the bound increases with increasing edge width. This is not surprising, since a smooth edge can be expected to be harder to localize in the presence of noise than a sharp edge, and this also agrees with the dependence of the CRB (26) on edge width for standard Gaussian noise. Second, for small edge width, the bound shows little dependence on position at the center of the image, but increases slightly when the edge approaches the boundaries of the image. This can be attributed to the truncation of some of the edge transition when the edge approaches the image boundaries. Third, for larger edge widths, the bound shows an asymmetric dependence on the edge position relative to the image center. This too can be explained by truncation of one side of the edge transition: however, because the noise is signal-dependent, the effect of truncating the bright side of the edge is opposite to that of truncating the dark side. Moreover, a similar effect of edge position is observed in the analytical CRB (27) for the NLF noise model, which also has signal-dependent noise level.

To further demonstrate the advantages of the GCRB, we investigate in the next experiment the ability of a generative model to capture the complex measurements distribution and produce an accurate lower bound. To this

end, we compare, in the context of the edge detection problem, the three noise models: WGN, NLF, and NoiseFlow. We do so for Device=2 (Samsung) (Fig. 3 at ISO level 100). For a quantitatively meaningful comparison, we set the parameters  $\sigma^2$ ,  $\alpha$ , and  $\delta$  of the analytical noise models to the maximum likelihood estimates obtained from the noisy images that were used to train NoiseFlow [6]. These noisy images are taken from the base SSID dataset [31], and were preprocessed as in NoiseFlow.

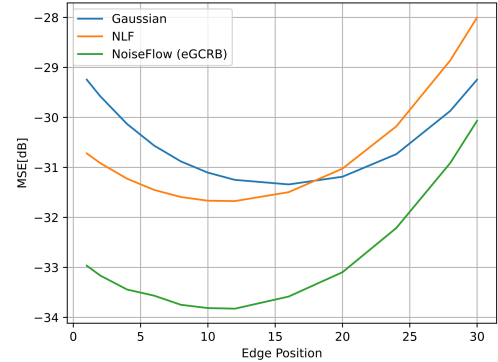


Fig. 13: Lower bound on edge position using different measurement noise models for Device=2 at ISO 100 and edge width 8 pixels.

Fig. 13 shows that (i) the WGN model misses altogether the asymmetric behavior of the bound with respect to edge position; and (ii) both Gaussian noise models have CRBs larger than the eGCRB. Both (i) and (ii) are to be expected, since the WGN model misses the signal-dependence of the noise, and independent Gaussian noise yields the largest CRB for given noise variance [35]. Finally, note the substantial difference between the eGCRB for Device=2 (in Fig. 13) and the eGCRB for Device=0 in Fig. 12 for the same edge width of 8 and ISO 100. This again demonstrates the unique ability of the GCRB to provide device-dependent bounds. Overall, these results illustrate the importance of a learned model to capture the complexity of the measurement distribution and obtain an accurate lower bound.

## VI. CONCLUSIONS AND FUTURE WORK

In this paper we use for the first time a generative model to obtain a data-driven estimate of the Cramer-Rao bound, which does not require access to an analytical model of the measurement probability distribution. Specifically, we used a normalizing flow and showed that this generative model provides the same CRB as measurement distribution if the generator is well-trained. Moreover, we bounded the inaccuracy due to the use of an empirical mean for the well-trained case. We validated the performance of this approach on two simple signal models with known ground-truth CRBs, and investigated the error of the GCRB due to imperfect learning and the use of an empirical mean. We also studied the GCRB on two image



processing tasks, with a complex learned measurement model. The results demonstrate two advantages of the GCRB: the ability to obtain a performance bound for complex measurement distributions without an analytical model; and the ability to obtain a device-specific bound. Questions for future research include quantifying the impacts of the limited representation power of the generative model and a limited training data set on the accuracy of the GCRB.

## REFERENCES

- [1] C Radhakrishna Rao. Information and the accuracy attainable in the estimation of statistical parameters. *Reson. J. Sci. Educ.*, 20:78–90, 1945.
- [2] Steven M Kay. *Fundamentals of statistical signal processing*. Prentice Hall PTR, 1993.
- [3] Harry L Van Trees. *Detection, estimation, and modulation theory, part I: detection, estimation, and linear modulation theory*. John Wiley & Sons, 2004.
- [4] Harry L Van Trees. *Optimum array processing: Part IV of detection, estimation, and modulation theory*. John Wiley & Sons, 2004.
- [5] Amer Catovic and Zafer Sahinoglu. The cramer-rao bounds of hybrid toa/rss and tdoa/rss location estimation schemes. *IEEE Communications Letters*, 8(10):626–628, 2004.
- [6] Abdelrahman Abdelhamed, Marcus A Brubaker, and Michael S Brown. Noise flow: Noise modeling with conditional normalizing flows. In *Proceedings of the IEEE/CVF International Conference on Computer Vision*, pages 3165–3173, 2019.
- [7] Joseph Carmack, Amit Bhatia, Josh Robinson, John Majewski, and Scott Kuzdeba. Neural network generative models for radio frequency data. In *2021 IEEE 12th Annual Ubiquitous Computing, Electronics & Mobile Communication Conference (UEMCON)*, pages 0577–0582. IEEE, 2021.
- [8] Yang Yang, Yang Li, Wuxiong Zhang, Fei Qin, Pengcheng Zhu, and Cheng-Xiang Wang. Generative-adversarial-network-based wireless channel modeling: Challenges and opportunities. *IEEE Communications Magazine*, 57(3):22–27, 2019.
- [9] Ian Goodfellow, Jean Pouget-Abadie, Mehdi Mirza, Bing Xu, David Warde-Farley, Sherjil Ozair, Aaron Courville, and Yoshua Bengio. Generative adversarial nets. In *Advances in neural information processing systems*, pages 2672–2680, 2014.
- [10] Durk P Kingma and Prafulla Dhariwal. Glow: Generative flow with invertible 1x1 convolutions. In S. Bengio, H. Wallach, H. Larochelle, K. Grauman, N. Cesa-Bianchi, and R. Garnett, editors, *Advances in Neural Information Processing Systems*, volume 31. Curran Associates, Inc., 2018.
- [11] Aaron Oord, Yazhe Li, Igor Babuschkin, Karen Simonyan, Oriol Vinyals, Koray Kavukcuoglu, George Driessche, Edward Lockhart, Luis Cobo, Florian Stimberg, et al. Parallel wavenet: Fast high-fidelity speech synthesis. In *International conference on machine learning*, pages 3918–3926. PMLR, 2018.
- [12] Yang Yang, Yang Li, Wuxiong Zhang, Fei Qin, Pengcheng Zhu, and Cheng-Xiang Wang. Generative-adversarial-network-based wireless channel modeling: Challenges and opportunities. *IEEE Communications Magazine*, 57(3):22–27, 2019.
- [13] Ivan Kobyzev, Simon Prince, and Marcus Brubaker. Normalizing flows: An introduction and review of current methods. *IEEE Transactions on Pattern Analysis and Machine Intelligence*, 2020.
- [14] George Papamakarios, Eric Nalisnick, Danilo Jimenez Rezende, Shakir Mohamed, and Balaji Lakshminarayanan. Normalizing flows for probabilistic modeling and inference. *Journal of Machine Learning Research*, 22(57):1–64, 2021.
- [15] Hai Victor Habi. Generative cramer rao bound. <https://github.com/haihabi/GenerativeCRB>, 2022.
- [16] Erich L Lehmann and George Casella. *Theory of point estimation*. Springer Science & Business Media, 2006.
- [17] Adam Paszke, Sam Gross, Francisco Massa, Adam Lerer, James Bradbury, Gregory Chanan, Trevor Killeen, Zeming Lin, Natalia Gimelshein, Luca Antiga, et al. Pytorch: An imperative style, high-performance deep learning library. *Advances in neural information processing systems*, 32:8026–8037, 2019.
- [18] S.A. Kassam and H.V. Poor. Robust techniques for signal processing: A survey. *Proceedings of the IEEE*, 73(3):433–481, 1985.
- [19] Gabor Lugosi and Shahar Mendelson. Robust multivariate mean estimation: the optimality of trimmed mean. *The Annals of Statistics*, 49(1):393–410, 2021.
- [20] Eunho Yang, Aurélie C Lozano, and Aleksandr Aravkin. A general family of trimmed estimators for robust high-dimensional data analysis. *Electronic Journal of Statistics*, 12(2):3519–3553, 2018.
- [21] Holden Lee, Chirag Pabbaraju, Anish Prasad Sevekari, and Andrej Risteski. Universal approximation using well-conditioned normalizing flows. *Advances in Neural Information Processing Systems*, 34, 2021.
- [22] Alexandre Verine, Benjamin Negrevergne, Fabrice Rossi, and Yann Chevaleyre. On the expressivity of bi-lipschitz normalizing flows. *arXiv preprint arXiv:2107.07232*, 2021.
- [23] Zhifeng Kong and Kamalika Chaudhuri. The expressive power of a class of normalizing flow models. In *International Conference on Artificial Intelligence and Statistics*, pages 3599–3609. PMLR, 2020.
- [24] Zhifeng Kong and Kamalika Chaudhuri. Universal approximation of residual flows in maximum mean discrepancy. In *ICML Workshop on Invertible Neural Networks, Normalizing Flows, and Explicit Likelihood Models*, 2021.
- [25] Željko Kereta and Timo Klock. Estimating covariance and precision matrices along subspaces. *Electronic Journal of Statistics*, 15(1):554–588, 2021.
- [26] Andreas Lugmayr, Martin Danelljan, Luc Van Gool, and Radu Timofte. Srfow: Learning the super-resolution space with normalizing flow. In *European Conference on Computer Vision*, pages 715–732. Springer, 2020.
- [27] Conor Durkan, Artur Bekasov, Iain Murray, and George Papamakarios. Cubic-spline flows. *arXiv preprint arXiv:1906.02145*, 2019.
- [28] Alessandro Foi, Mejdi Trimeche, Vladimir Katkovnik, and Karen Egiazarian. Practical poissonian-gaussian noise modeling and fitting for single-image raw-data. *IEEE Transactions on Image Processing*, 17(10):1737–1754, 2008.
- [29] Jiachao Zhang and Keigo Hirakawa. Improved denoising via poisson mixture modeling of image sensor noise. *IEEE Transactions on Image Processing*, 26(4):1565–1578, 2017.
- [30] Jingwen Chen, Jiawei Chen, Hongyang Chao, and Ming Yang. Image blind denoising with generative adversarial network based noise modeling. In *Proceedings of the IEEE Conference on Computer Vision and Pattern Recognition*, pages 3155–3164, 2018.
- [31] Abdelrahman Abdelhamed, Stephen Lin, and Michael S Brown. A high-quality denoising dataset for smartphone cameras. In *Proceedings of the IEEE Conference on Computer Vision and Pattern Recognition*, pages 1692–1700, 2018.
- [32] Diederik P Kingma and Jimmy Ba. Adam: A method for stochastic optimization. *arXiv preprint arXiv:1412.6980*, 2014.
- [33] Dan Hendrycks and Kevin Gimpel. Gaussian error linear units (gelus). *arXiv preprint arXiv:1606.08415*, 2016.
- [34] [https://github.com/BorealisAI/noise\\_flow](https://github.com/BorealisAI/noise_flow).
- [35] Petre Stoica and Prabhu Babu. The gaussian data assumption leads to the largest cramer-rao bound [lecture notes]. *IEEE Signal Processing Magazine*, 28(3):132–133, 2011.
- [36] Kaare Brandt Petersen, Michael Syskind Pedersen, et al. The matrix cookbook. *Technical University of Denmark*, 7(15):510, 2008.
- [37] Laurent Dinh, Jascha Sohl-Dickstein, and Samy Bengio. Density estimation using real nvp. *arXiv preprint arXiv:1605.08803*, 2016.
- [38] Ian Goodfellow, Yoshua Bengio, and Aaron Courville. *Deep learning*. MIT press, 2016.

## APPENDIX

## A. Score Vector Derivation

1) *Score Vector Hybrid Version:* We show a detailed derivation of the score vector expressed in terms of both  $\nu$  and  $G$ . We start by splitting (5) into

$$\mathbf{s}_\theta(\mathbf{z}) = \frac{\partial \log p_{\mathbf{z}}(\nu(\gamma; \theta))}{\partial \theta} \Big|_{\gamma=G(\mathbf{z}; \theta)} + \frac{\partial \log |\det \mathbf{J}_\nu(\gamma; \theta)|}{\partial \theta} \Big|_{\gamma=G(\mathbf{z}; \theta)}. \quad (31)$$

Applying the chain rule to the first term yields

$$\frac{\partial \log p_{\mathbf{z}}(\nu(\gamma; \theta))}{\partial \theta} = \frac{\partial \nu(\gamma; \theta)}{\partial \theta}^T \frac{\partial \log p_{\mathbf{z}}(\mathbf{z})}{\partial \mathbf{z}}. \quad (32)$$

For the second term

$$\begin{aligned} \frac{\partial \log |\det \mathbf{J}_\nu(\gamma; \theta)|}{\partial \theta_i} &= \\ \frac{1}{2} \frac{\partial \log \det [\mathbf{J}_\nu^T(\gamma; \theta) \mathbf{J}_\nu(\gamma; \theta)]}{\partial \theta_i} &= \\ \text{Tr} \left( \mathbf{J}_\nu^{-1}(\gamma; \theta) \frac{\partial \mathbf{J}_\nu(\gamma; \theta)}{\partial \theta_i} \right), \end{aligned} \quad (33)$$

where the second equality follows from the identity [36]

$$\frac{\partial \log \det B(t)}{\partial t} = \text{Tr} \left( B^{-1}(t) \frac{\partial B(t)}{\partial t} \right)$$

for positive-definite matrix  $B(t) = A^T(t)A(t)$  where  $A(t) \triangleq \mathbf{J}_\nu^{-1}(\gamma; (\theta_1, \dots, \theta_{i-1}, t, \theta_{i+1}, \theta_k))$ . Substituting (32) and (33) into (31) yields (6).

2) *Score Vector Generator Version:* We derive an alternative expression for the score vector, in terms of  $G$  only. We begin with the defining identity

$$\nu(G(\mathbf{z}; \theta); \theta) = \mathbf{z}. \quad (34)$$

Taking a derivative w.r.t  $\theta$  results in

$$\begin{aligned} 0 &= \frac{\partial \nu(G(\mathbf{z}; \theta); \theta)}{\partial \theta} = \\ &= \frac{\partial \nu(\gamma; \theta)}{\partial \theta} \Big|_{\gamma=G(\mathbf{z}; \theta)} + \mathbf{J}_\nu(G(\mathbf{z}; \theta); \theta) \frac{\partial G(\mathbf{z}; \theta)}{\partial \theta} \\ &= \frac{\partial \nu(\gamma; \theta)}{\partial \theta} \Big|_{\gamma=G(\mathbf{z}; \theta)} + \mathbf{J}_G^{-1}(\mathbf{z}; \theta) \frac{\partial G(\mathbf{z}; \theta)}{\partial \theta}. \end{aligned}$$

This provides the useful identity

$$\frac{\partial \nu(\gamma; \theta)}{\partial \theta} \Big|_{\gamma=G(\mathbf{z}; \theta)} = -\mathbf{J}_G^{-1}(\mathbf{z}; \theta) \frac{\partial G(\mathbf{z}; \theta)}{\partial \theta}. \quad (35)$$

We use (35) directly to replace the first term in (6), eliminating its dependence on  $\nu$ .

Consider now the second term in (31).

$$\begin{aligned} [\mathbf{w}(\mathbf{z}; \theta)]_i &\triangleq \frac{\partial \log |\det \mathbf{J}_\nu(\gamma; \theta)|}{\partial \theta_i} = \\ \frac{\partial \log |\det \mathbf{J}_G(\nu(\gamma; \theta); \theta)|^{-1}}{\partial \theta_i} &= \\ - \frac{\partial \log |\det \mathbf{J}_G(\nu(\gamma; \theta); \theta)|}{\partial \theta_i} &= \\ - \text{Tr} \left( \mathbf{J}_G^{-1}(\nu(\gamma; \theta); \theta) \frac{\partial \mathbf{J}_G(\nu(\gamma; \theta); \theta)}{\partial \theta_i} \right), \end{aligned} \quad (36)$$

where the first equality follows directly from the inverse function theorem  $\mathbf{J}_\nu(\gamma; \theta) = \mathbf{J}_G^{-1}(\nu(\gamma; \theta); \theta)$  and the third follows from (33) upon replacing  $\nu$  by  $G$ . The second factor under the trace in (36) is

$$\frac{\partial \mathbf{J}_G(\nu(\gamma; \theta); \theta)}{\partial \theta_i} = \frac{\partial \mathbf{J}_G(\xi; \theta)}{\partial \theta_i} + \mathbf{M}_i(\xi) \Big|_{\xi=\nu(\gamma; \theta)}, \quad (37)$$

where the  $kl$  element of  $\mathbf{M}_i$  is

$$[\mathbf{M}_i(\xi)]_{kl} = \frac{\partial [\mathbf{J}_G(\xi; \theta)]_{kl}}{\partial \xi}^T \frac{\partial \nu(\gamma; \theta)}{\partial \theta_i} \Big|_{\gamma=G(\xi; \theta)}.$$

Then using (35) yields

$$[\mathbf{M}_i(\xi)]_{kl} = - \frac{\partial [\mathbf{J}_G(\xi; \theta)]_{kl}}{\partial \xi}^T \mathbf{J}_G^{-1}(\xi; \theta) \frac{\partial G(\xi; \theta)}{\partial \theta}. \quad (38)$$

Next, we combine (36), (37) and (38) to obtain

$$\begin{aligned} [\mathbf{w}(\mathbf{z}; \theta)]_i &\triangleq \frac{\partial \log |\det \mathbf{J}_\nu(\gamma; \theta)|}{\partial \theta_i} \Big|_{\gamma=G(\mathbf{z}; \theta)} = \\ - \text{Tr} \left( \mathbf{J}_G^{-1}(\nu(\gamma; \theta); \theta) \frac{\partial \mathbf{J}_G(\nu(\gamma; \theta); \theta)}{\partial \theta_i} \right) &\Big|_{\gamma=G(\mathbf{z}; \theta)} \\ = - \text{Tr} \left( \mathbf{J}_G^{-1}(\mathbf{z}; \theta) \frac{\partial \mathbf{J}_G(\nu(\gamma; \theta); \theta)}{\partial \theta_i} \right) &\Big|_{\gamma=G(\mathbf{z}; \theta)} \\ = - \text{Tr} \left( \mathbf{J}_G^{-1}(\mathbf{z}; \theta) \left( \frac{\partial \mathbf{J}_G(\mathbf{z}; \theta)}{\partial \theta_i} + \mathbf{M}_i(\mathbf{z}) \right) \right). \end{aligned}$$

Finally, the score vector is given by

$$\mathbf{s}_\theta(\mathbf{z}) = - \frac{\partial G(\mathbf{z}; \theta)}{\partial \theta}^T \mathbf{J}_G^{-T}(\mathbf{z}; \theta) \frac{\partial \log p_{\mathbf{z}}(\mathbf{z})}{\partial \mathbf{z}} - \mathbf{w}(\mathbf{z}; \theta). \quad (39a)$$

$$[\mathbf{w}(\mathbf{z}; \theta)]_i = \text{Tr} \left( \mathbf{J}_G^{-1}(\mathbf{z}; \theta) \frac{\partial \mathbf{J}_G(\mathbf{z}; \theta)}{\partial \theta_i} \right) + \text{Tr} \left( \mathbf{J}_G^{-1}(\mathbf{z}; \theta) \mathbf{M}_i(\mathbf{z}) \right). \quad (39b)$$

$$[\mathbf{M}_i(\mathbf{z})]_{kl} = - \frac{\partial [\mathbf{J}_G(\mathbf{z}; \theta)]_{kl}}{\partial \mathbf{z}} \mathbf{J}_G^{-1}(\mathbf{z}; \theta) \frac{\partial G(\mathbf{z}; \theta)}{\partial \theta}. \quad (39c)$$

Examining the various derivatives appearing in (39), it follows that for the generator score vector (39) to be well-defined, it suffices to require that  $G \in C^2$ . Thanks to the defining relation (34) between  $G$  and  $\nu$ , which induces the equivalence between (39) and (6), it follows that the same condition,  $G \in C^2$ , suffices for (6) to be well-defined too.

## B. Proof of Thm 2.3

*Proof:*

$$\begin{aligned} \mathbf{F}_R(\theta) &= \int_{\hat{\mathbf{r}}} \frac{\partial \mathbf{L}_R(\theta)}{\partial \theta} \left[ \frac{\partial \mathbf{L}_R(\theta)}{\partial \theta} \right]^T p_R(\mathbf{r}; \theta) d\mathbf{r} + \epsilon_t(\theta) \\ &= \int_{\hat{\mathbf{r}}} \frac{\partial \mathbf{L}_\Gamma(\theta)}{\partial \theta} \left[ \frac{\partial \mathbf{L}_\Gamma(\theta)}{\partial \theta} \right]^T p_\Gamma(\gamma; \theta) d\gamma + \epsilon_t(\theta) \\ &= \int_{\mathcal{Z}} \mathbf{s}_\theta(\mathbf{z}) \mathbf{s}_\theta(\mathbf{z})^T p_{\mathbf{Z}}(\mathbf{z}) d\mathbf{z} + \epsilon_t(\theta) \\ &= \hat{\mathbf{F}}_G(\theta) + \epsilon_t(\theta) = \mathbb{E}_{\mathbf{z}} [\overline{\mathbf{F}}_G(\theta)] + \epsilon_t(\theta), \end{aligned}$$

where  $\epsilon_t(\theta)$  is defined in (16) and  $\mathcal{Z} \triangleq G^{-1}(\hat{\Upsilon}; \theta)$  is the pre-image of  $\hat{\Upsilon}$  under  $G$ . The first equality follows by writing out the expectation in the definition (1) of the FIM as an integral, and splitting the domain of integration as  $\Upsilon = \hat{\Upsilon} \cup (\Upsilon \setminus \hat{\Upsilon})$ . The second equality follows from Assumption 2.4 of a well-trained generator, and the third follows using the Law of the Unconscious Statistician (LOTUS) to replace the expected value respect to  $\Gamma$  restricted to  $\hat{\Upsilon}$  by that with respect to  $\mathbf{z}$  restricted to  $\mathcal{Z}$ . In the last step, we use the fact that  $\hat{\mathbf{z}}$  is sampled i.i.d when computing the empirical mean. ■

### C. Score Vector Mean and Bound

The following result is used in the proof of the sampling error Theorem 2.2 in the next subsection.

*Lemma 1.1:* Let  $\mathbf{s}_\theta(\mathbf{z})$  be a score vector computed using a well-trained (11) generator  $G$  and it's inverse  $\nu$  assuming  $\hat{\Upsilon} = \Upsilon$ . Then  $\mathbb{E}_{\mathbf{z}}[\mathbf{s}_\theta(\mathbf{z})] = 0$ .

*Proof:* By definition,

$$\mathbb{E}_{\mathbf{z}}[\mathbf{s}_\theta(\mathbf{z})] = \mathbb{E}_{\mathbf{z}} \left[ \frac{\partial \log p_{\Gamma}(\Gamma; \theta)}{\partial \theta} \Big|_{\Gamma=G(\mathbf{z}; \theta)} \right]$$

First using LOTUS we replace the expected value w.r.t  $\mathbf{z}$  by that with respect to  $\Gamma$ .

$$\mathbb{E}_{\mathbf{z}}[\mathbf{s}_\theta(\mathbf{z})] = \mathbb{E}_{\Gamma} \left[ \frac{\partial \log p_{\Gamma}(\Gamma; \theta)}{\partial \theta} \right],$$

Next, we use the well-trained Assumption 2.4 which results in:

$$\mathbb{E}_{\Gamma} \left[ \frac{\partial \log p_{\Gamma}(\Gamma; \theta)}{\partial \theta} \right] = \mathbb{E}_{\mathbf{R}} \left[ \frac{\partial \log p_{\mathbf{R}}(\mathbf{R}; \theta)}{\partial \theta} \right] = 0,$$

where the second equality follows from the CRB regularity condition on  $p_{\mathbf{R}}(\mathbf{r}; \theta)$  [2]. ■

*Lemma 1.2:* Let  $\mathbf{s}_\theta(\mathbf{z})$  be a score vector computed using a well-trained (11) generator  $G$  and it's inverse  $\nu$ . Then  $\|\mathbf{s}_\theta(\mathbf{z})\| \leq C_s(\theta)$ .

*Proof:* The generated samples  $\gamma = G(\mathbf{z}; \theta) \in \hat{\Upsilon}$  retained after the trimming process correspond to  $\mathbf{z} \in \mathcal{Z}$ , where the set  $\mathcal{Z} \triangleq G^{-1}(\hat{\Upsilon}; \theta)$  is the pre-image of  $\hat{\Upsilon}$  under  $G$ . Because  $\hat{\Upsilon}$  is a compact set in metric space  $\mathbb{R}^d$  (Assumption A.7) and  $G^{-1} = \nu : \mathbb{R}^d \rightarrow \mathbb{R}^d$  is a continuous mapping, it follows that as the image of a compact set by a continuous mapping,  $\mathcal{Z}$  is a compact set. Next, because  $G \in C^2$  and  $G$  is a diffeomorphism wrt to  $\mathbf{z}$ , it follows that each of the components  $\mathbf{s}_\theta(\mathbf{z})$  is a continuous function of  $\mathbf{z}$  on the compact set  $\mathcal{Z}$ . Hence (by pseudocompactness)  $\mathbf{s}_\theta(\mathbf{z})$  is bounded componentwise, and thus also in norm:  $\|\mathbf{s}_\theta(\mathbf{z})\| \leq C_s(\theta)$ . ■

### D. Sampling Convergence Bound

We provide a proof for the sampling error Theorem 2.2. First we present a bound on the estimation of the precision matrix (inverse of the a covarinace matrix).

*Theorem 1.3:* (Theorem 13 in [25], specialized for  $\mathbb{E}[\mathbf{x}] = 0$ .) Let  $\mathbf{x} \in \mathbb{R}^D$  be a random vector with  $\mathbb{E}[\mathbf{x}] = 0$  and covariance matrix  $\Sigma = \mathbb{E}[\mathbf{x}\mathbf{x}^T]$ . Assume

$\|\mathbf{A}\Sigma^{-1}\mathbf{x}\|_2 \leq C_A$ ,  $\|\mathbf{B}\Sigma^{-1}\mathbf{x}\|_2 \leq C_B$ ,  $\|\sqrt{\Sigma^{-1}}\mathbf{x}\|_2 \leq C_x$  almost surely, where  $\mathbf{A} \in \mathbb{R}^{d_1 \times D}$ ,  $\mathbf{B} \in \mathbb{R}^{d_2 \times D}$  are known matrices. Let  $\mathbf{x}_1, \dots, \mathbf{x}_m$  be a set of  $m$  independent copies of  $\mathbf{x}$  with  $\hat{\Sigma} = \frac{1}{m} \sum_{j=1}^m \mathbf{x}_j \mathbf{x}_j^T$  the finite sample estimator of  $\Sigma$ . Then there exist absolute constants  $C_1 > 0$  and  $C_2 > 0$  such that provided  $m > C_1(1+u)C_x^2$ , we have with probability at least  $1 - \exp(-u)$  for any  $u > 0$  that

$$\left\| \mathbf{A} \left( \hat{\Sigma}^{-1} - \Sigma^{-1} \right) \mathbf{B}^T \right\|_F \leq C_2 C_A C_B \sqrt{\frac{1+u}{m}}.$$

*Proof:* (Sketch, for Theorem 1.3) The proof of Theorem 13 in [25] starts with

$$\left\| \mathbf{A}_{\Sigma} \left( \hat{\Sigma} - \Sigma \right) \mathbf{B}_{\Sigma}^T \right\| \leq \left\| \mathbf{A}_{\Sigma} \left( \tilde{\Sigma} - \Sigma \right) \mathbf{B}_{\Sigma}^T \right\| + \epsilon, \quad (40)$$

where  $\tilde{\Sigma} = \frac{1}{m} \sum_{j=1}^m (\mathbf{x}_j - \mathbb{E}[\mathbf{x}]) (\mathbf{x}_j - \mathbb{E}[\mathbf{x}])^T$  and  $\epsilon$  is some high order terms. With our definitions of  $\hat{\Sigma}$  and  $\mathbb{E}[\mathbf{x}] = 0$  we have that  $\hat{\Sigma} = \tilde{\Sigma}$  and therefore (40) holds with equality for  $\epsilon = 0$ . The rest of the proof follows [25]. ■

*Proof:* (of Theorem 2.2) Lemma 1.2 provides Result (i) of the theorem, that  $\|\mathbf{s}_\theta(\mathbf{z})\| \leq C_s(\theta)$ . Next, Assumption 2.3 and  $\epsilon_r = 0$  imply that  $\hat{\Upsilon} = \Upsilon$ , so that by Lemma 1.1 we have  $\mathbb{E}_{\mathbf{z}}[\mathbf{s}_\theta(\mathbf{z})] = 0$ . It follows that Theorem 1.3 is applicable to the score vector  $\mathbf{x} = \mathbf{s}_\theta(\mathbf{z})$  satisfying  $\mathbb{E}[\mathbf{x}] = 0$  and  $\|\mathbf{x}\| \leq C_s(\theta)$ . Making the identifications  $\Sigma = F_G$ , and  $\hat{\Sigma} = \overline{F}_G(\theta)$  and setting  $\mathbf{A} = \mathbf{B} = \mathbf{I}$ ,  $C_A = C_B = \|\Sigma^{-1}\|_F C_s(\theta)$  results in:

$$\left\| \overline{F}_G(\theta)^{-1} - F_G^{-1}(\theta) \right\|_F \leq C_2 \|F_G^{-1}(\theta)\|_F^2 C_s^2(\theta) \sqrt{\frac{1+u}{m}}.$$

■

### E. Flow Layers Overview

**Affine Coupling** The affine coupling flow layer [37] is a powerful transformation that enables efficient computation of the forward function, the inverse function and the log-determinant. Let  $\mathbf{z}_n = (\mathbf{z}_n^A, \mathbf{z}_n^B)$  be a partition of the components of the vector  $\mathbf{z}_n$ . Then the affine coupling layer is defined as follows:

$$\mathbf{z}_{n+1} = \left( \exp(f_{\omega_n, s}^n(\mathbf{z}_n^B)) \mathbf{z}_n^A + f_{\omega_n, b}^n(\mathbf{z}_n^B), \mathbf{z}_n^B \right), \quad (41)$$

where  $f_{\omega_n, s}^n(\mathbf{z}_n^B)$  and  $f_{\omega_n, b}^n(\mathbf{z}_n^B)$  are the scale and bias neural networks of the  $n^{th}$  transformation, respectively, each parametrized by the learnable parameter vector  $\omega_n$ . Note that the affine coupling layer applies an affine transformation to one of the disjoint blocks of  $\mathbf{z}_n$ , whereas the second block is simply passed forward to the next flow layer. The inverse of (41) is given by

$$\mathbf{z}_n^A = \frac{\mathbf{z}_{n+1}^A - f_{\omega_n, b}^n(\mathbf{z}_{n+1}^B)}{\exp(f_{\omega_n, s}^n(\mathbf{z}_{n+1}^B))}, \quad \mathbf{z}_n^B = \mathbf{z}_{n+1}^B,$$

and the log-determinant term is  $\sum_i [f_{\omega_n, s}^n(\mathbf{z}_n^B)]_i$ . Note that  $f_{\omega_n, b}^n$  and  $f_{\omega_n, s}^n$  can be an arbitrary complex neural networks, and the affine coupling layer is invertible thanks to its structure.

**Affine Inject** The Affine Injector conditional flow layer [26] enables direct information transfer from the conditioning parameter vector to the flow branch that directly affects the entire input vector  $\mathbf{z}_n$ . This is achieved by controlling the scaling and bias using only the conditioning parameter vector  $\boldsymbol{\theta}$ :

$$\mathbf{z}_{n+1} = \exp(f_{\omega_n, s}^n(\boldsymbol{\theta})) \mathbf{z}_n + f_{\omega_n, b}^n(\boldsymbol{\theta}), \quad (42)$$

where  $f_{\omega_n, b}^n$  and  $f_{\omega_n, s}^n$  are the scale and bias neural networks of the  $n^{th}$  transformation, respectively. The inverse and log-determinant of (42) are given by  $\mathbf{z}_n = \exp(-f_{\omega_n, s}^n(\boldsymbol{\theta})) (\mathbf{z}_{n+1} - f_{\omega_n, b}^n(\boldsymbol{\theta}))$  and  $\sum_i f_{\omega_n, s}^n(\boldsymbol{\theta})_i$ . Note that  $f_{\omega_n, b}^n$  and  $f_{\omega_n, s}^n$  can be an arbitrary complex neural networks.

**Spline Flow** The spline flow [27] uses monotonic cubic splines to extend the affine coupling layer [37]. Specifically, a spline flow is defined as

$$\mathbf{z}_{n+1}^B = g(\mathbf{z}_n^B, f_{\omega_n}^n(\mathbf{z}_n^A)), \quad \mathbf{z}_{n+1}^A = \mathbf{z}_n^A,$$

where  $\mathbf{z}_n = [\mathbf{z}_n^A, \mathbf{z}_n^B]$  is the splitting of vector  $\mathbf{z}_n$  into two parts,  $g$  is a monotonic cubic spline and  $f_{\omega_n}^n$  is an arbitrary neural network that generates the spline parameters.

**Invertible Matrix Product** The so-called  $1 \times 1$  convolution has been proposed as a flow layer [10], with an LU decomposition of the corresponding matrix to reduce the cost of computing the log-determinant. The same can be done for matrix multiplication:

$$\mathbf{z}_{n+1} = \mathbf{W} \mathbf{z}_n, \quad (43)$$

where  $\mathbf{W} = \mathbf{P} \mathbf{L} (\mathbf{U} + \text{diag}(\mathbf{s}))$ ,  $\mathbf{P}$  is a fixed permutation matrix,  $\mathbf{L}$ ,  $\mathbf{U}$  are trainable lower and upper triangular matrices with ones and zeros on the diagonal, respectively, and  $\mathbf{s}$  is a trainable vector with non-zero entries. The inverse and log-determinant term for the layer of (43) are given by  $\mathbf{z}_n = \mathbf{W}^{-1} \mathbf{z}_{n+1}$  and  $\sum_i \mathbf{s}_i$ , respectively.

**Activation Normalization** The activation normalization flow layer [10] perform an affine transformation of the channel using a scale and bias. The scale and bias are initialized using the statics of the first training batch such that each output of this flow step will have zero mean and unit variance given an initial minibatch of data. Then the scale and bias are treated as regular trainable parameters. Denoting the scale and bias vectors by  $\mathbf{s}$  and  $\mathbf{b}$ , respectively, the activation normalization is defined as

$$\mathbf{z}_{n+1} = \mathbf{s} \odot \mathbf{z}_n + \mathbf{b}. \quad (44)$$

The inverse of (44) is given by  $\mathbf{z}_n = \frac{1}{\mathbf{s}} \odot (\mathbf{z}_{n+1} - \mathbf{b})$  and the log-determinant term is  $\sum_i [\mathbf{s}]_i$ .

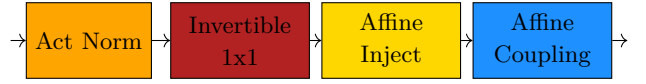


Fig. 14: Basic Flow Block

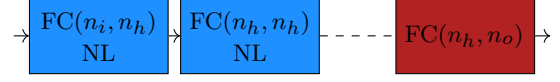


Fig. 15: Multilayer Perceptron

#### F. CRB for the Scale Non-Gaussian Example

Let  $r = \theta y$  then using transformation of variables  $p_R(r) = p_y(\frac{r}{\theta}) \theta^{-1}$  which results in:

$$p_R(r) = \frac{1}{\sqrt{2\pi\sigma^2}} \frac{3r^2}{\theta^3} \cdot \exp\left(-\frac{1}{2\sigma^2} \left(\frac{r}{\theta}\right)^6\right)$$

Then the NNL function of  $p_R(r)$  is given by:

$$L_R(\theta) = c + 3 \log(\theta) + \frac{1}{2\sigma^2} \left(\frac{r}{\theta}\right)^6$$

where  $c$  is some constant. Taking a derivative wrt  $\theta$ :

$$\frac{\partial L_R(\theta)}{\partial \theta} = \frac{3}{\theta} \left(1 - \frac{1}{\sigma^2} \left(\frac{r}{\theta}\right)^6\right)$$

The FIM is then given by:

$$\begin{aligned} F_R(\theta) &= \mathbb{E}_R \left[ \left( \frac{\partial L_R(\theta)}{\partial \theta} \right)^2 \right] = \frac{9}{\theta^2} \mathbb{E}_R \left[ \left( 1 - \frac{1}{\sigma^2} \left( \frac{r}{\theta} \right)^6 \right)^2 \right] \\ &= \frac{9}{\theta^2} \left( 1 - \frac{2}{\sigma^2} \mathbb{E}_R \left[ \left( \frac{r}{\theta} \right)^6 \right] + \frac{1}{\sigma^4} \mathbb{E}_R \left[ \left( \frac{r}{\theta} \right)^{12} \right] \right) = 18\theta^{-2}. \end{aligned}$$

**1) Scale Model Optimal Generator Compare:** We show that  $\Gamma(\theta) = G(z) = \theta z^{1/3}$  is an optimal generator that produces  $p_R(r)$ :

$$\begin{aligned} p_\Gamma(\gamma) &= p_Z \left( \left( \frac{\gamma}{\theta} \right)^3 \right) 3 \frac{\gamma^2}{\theta} \\ &= \frac{1}{\sqrt{2\pi\sigma^2}} \frac{3\gamma^2}{\theta^3} \cdot \exp\left(-\frac{1}{2\sigma^2} |\gamma|^6 \theta^{-6}\right) = p_R(\gamma). \end{aligned}$$

where  $\mathbf{z} \sim \mathcal{N}(0, 1)$  and  $\nu(\gamma) = \left(\frac{\gamma}{\theta}\right)^3$  is the inverse of the optimal generator.

#### G. Edge Detection FIM and CRB

In this section, we provide the FIM and CRB for the edge position estimation problem defined in Sec. IV-B.2 with two noise models: WGN and NLF.

**1) WGN:** Because  $\mathbf{V}_{ijc} \sim \mathcal{N}(0, \sigma^2)$  is Gaussian Noise, the CRB for general Gaussian noise [2] is applicable. The FIM is given by:

$$\mathbf{F}(\theta_p) = \frac{1}{\sigma^2} \text{Vec}(\mathbf{D}_H(\theta_p))^T \text{Vec}(\mathbf{D}_H(\theta_p)), \quad (45)$$

$$[\mathbf{D}_H(\theta_p)]_{ijc} = \frac{\partial f_{ijc}(\theta_p)}{\partial \theta_p} = \frac{(p_c^h - p_c^l)}{e} s_i(\theta_p) (1 - s_i(\theta_p)).$$



Substituting into (45) yields

$$\begin{aligned} \mathbf{F}(\theta_p) &= \frac{1}{\sigma^2 e^2} \sum_i \sum_j \sum_c (p_c^h - p_c^l)^2 s_i(\theta_p)^2 (1 - s_i(\theta_p))^2, \\ &= \frac{h}{\sigma^2 e^2} \|\mathbf{p}^h - \mathbf{p}^l\|_2^2 \sum_i s_i(\theta_p)^2 (1 - s_i(\theta_p))^2, \end{aligned}$$

which provides upon inversion the CRB

$$\text{CRB}_W(\theta_p) = \frac{\sigma^2 e^2}{h \|\mathbf{p}^h - \mathbf{p}^l\|_2^2} \left( \sum_i s_i(\theta_p)^2 (1 - s_i(\theta_p))^2 \right)^{-1}.$$

**2) Noise Level Function:** Using the noise model  $\mathbf{V}_{ijc} \sim \mathcal{N}(0, \alpha^2 f_{ijc}(\theta_p) + \delta^2)$ , the CRB formula for general Gaussian noise is again applicable with FIM

$$\begin{aligned} \mathbf{F}(\theta_p) &= \text{Vec}(\mathbf{D}_H(\theta_p))^T \mathbf{C}(\theta_p)^{-1} \text{Vec}(\mathbf{D}_H(\theta_p)) \\ &\quad + \frac{1}{2} \text{Tr} \left( \left( \mathbf{C}(\theta_p)^{-1} \frac{\partial \mathbf{C}(\theta_p)}{\partial \theta_p} \right)^2 \right), \end{aligned} \quad (46)$$

where  $\mathbf{C}(\theta_p) = (\alpha \text{Vec}(\mathbf{H}(\theta_p)) + \delta) (\alpha \text{Vec}(\mathbf{H}(\theta_p)) + \delta)^T$ .

The first term of (46) is

$$\begin{aligned} T_1 &\triangleq \text{Vec}(\mathbf{D}_H(\theta_p))^T \mathbf{C}(\theta_p)^{-1} \text{Vec}(\mathbf{D}_H(\theta_p)), \\ &= \sum_i \sum_j \sum_c \frac{1}{\alpha^2 f_{ijc}(\theta_p) + \delta^2} \left( \frac{\partial f_{ijc}(\theta_p)}{\partial \theta_p} \right)^2. \end{aligned}$$

The second term is given by:

$$\begin{aligned} T_2 &\triangleq \frac{1}{2} \text{Tr} \left( \left( \mathbf{C}(\theta_p)^{-1} \frac{\partial \mathbf{C}(\theta_p)}{\partial \theta_p} \right)^2 \right), \\ &= \frac{1}{2} \sum_i \sum_j \sum_c \frac{\alpha^2}{(\alpha^2 f_{ijc}(\theta_p) + \delta^2)^2} \left( \frac{\partial f_{ijc}(\theta_p)}{\partial \theta_p} \right)^2. \end{aligned}$$

Combining  $T_1$  and  $T_2$  yields

$$\begin{aligned} \mathbf{F}(\theta_p) &= \sum_{i,j,c} \frac{\left( \frac{\partial f_{ijc}(\theta_p)}{\partial \theta_p} \right)^2}{\alpha^2 f_{ijc}(\theta_p) + \delta^2} \left( 1 + \frac{\alpha^2}{2(\alpha^2 f_{ijc}(\theta_p) + \delta^2)} \right), \\ &= \sum_{i,j,c} \frac{\alpha^2 (1 + 2f_{ijc}(\theta_p)) + 2\delta^2}{2(\alpha^2 f_{ijc}(\theta_p) + \delta^2)^2} \left( \frac{\partial f_{ijc}(\theta_p)}{\partial \theta_p} \right)^2, \end{aligned}$$

yielding upon inversion the CRB (27).

## H. Flow Parameters and Training Details

**1) Flow Step:** We use a CNF based on the Glow [10] architecture (see Section III). The architecture uses basic block (Fig. 14) that consists of the following consecutive layers: activation Normalization [10], 1x1 convolution [10], affine inject layer, and coupling layer [27], [37]. In both coupling and affine inject layers the parameter network generation is MLP (Section H.2) with different architectural choices for each problem.

**2) Multilayer Perceptron (MLP):** Several CNF layers (affine coupling, spline coupling, and affine inject) used throughout this work require a function to map the conditioning input to the layer parameters. We choose to implement these functions as a standard Multilayer Perceptron (MLP) [38] (Fig. 15), which is a sequence of fully connected layers with a non-linearity in between. Each fully connected layer consists of a matrix and a bias vector, which are optimized during training. The MLP we use is defined by five architectural choices: the input and output vector sizes  $n_o$  and  $n_i$ , which are chosen equal and defined by problem dimensions and flow layer; the number of hidden neurons  $n_h$ ; the number of layers  $n_{layers}$ , which is chosen differently for each of our examples; and the non-linear function. For the latter we chose the Sigmoid Linear Unit (SiLU) activation function [33], allowing the resulting normalizing flow and generator to satisfy our differentiability assumptions.<sup>2</sup> Note that the output layer of the MLP does not include a nonlinearity and that if  $n_{layers} = 1$ , the MLP will be degenerate to a single fully connected layer.

**3) Linear Gaussian Flow:** In the linear example, we use one flow block with affine coupling [37] (Appendix H.1). The MLP network (Appendix H.2) used in the flow step consists of one layer ( $n_{layer} = 1$ ). We use the normalizing flow above because it has sufficient expressive power for this example - in particular, it can represent an optimal generator for a linear Gaussian example. Since  $\mathbf{z} \sim \mathcal{N}(0, \mathbf{I})$ , we need to transform  $\mathbf{z}$  to  $\mathbf{z}_1 \sim \mathcal{N}(0, \mathbf{C}_{vv})$ , this is achievable using an invertible 1x1 convolution with weights  $W = L$ . Then, the effect of the parameter vector  $\theta$  can be represented using the Affine Inject with single layer MLP  $\mathbf{z}_{n+1} = \mathbf{A}\theta + \mathbf{z}_n$ . Note that we use a more complex normalizing flow than the optimal  $G(\mathbf{z}; \theta) = \mathbf{A}\theta + \mathbf{L}\mathbf{z}$ , in the sense that we have additional layers (affine coupling and act norm) and parameters, which may require more data for training.

**4) Scale Non-Gaussian Flow:** In the non-Gaussian scale example, we use two flow blocks with a cubic spline coupling [27]. We utilized the cubic spline coupling for its ability to locally model non-linear functions such as  $x^3$ , where in this example it would need to model  $x^{1/3}$ . Then the affine inject layer can scale the transformation by  $\theta$ , which simulates locally the required transformations. The MLP network (Appendix H.2) used in the flow step consists of five layers ( $n_{layer} = 5$ ) and 64 hidden neurons ( $n_h = 64$ ).

<sup>2</sup>We observed essentially identical results using a ReLU for the nonlinearity, which violates the differentiability assumptions at its "corner" at zero. The insensitivity of our scheme to this may be attributed to the fact that the ReLU is differentiable almost everywhere, so that sampling from continuous probability distributions, the likelihood of landing on the "corner" of any of the ReLUs in the network is zero.